HIGH THROUGHPUT CENTRIFUGE MICROFLUIDIC DEVICE FOR SIMULTANEOUS PARTICLE SEPARATION AND SOLUTION EXCHANGE

Nima Norouzy

A THESIS SUBMITTED TO THE FACULTY OF GRADUATE STUDIES IN PARTIAL FULFILLMENT OF THE REQUIREMENTS FOR THE DEGREE OF MASTER OF SCIENCE

GRADUATE PROGRAM IN MECHANICAL ENGINEERING

YORK UNIVERSITY

TORONTO, ONTARIO

December 2023

Abstract

Microfluidic centrifuge devices have gained increasing attention for point-of-need (PoN) sample preparation processes, e.g., in separation or solution exchange of various microparticles, bacteria, and mammalian cells. Yet, those devices capable of simultaneous solution exchange and particle separation are low in throughput (can operate at up to 2 mL/min), hindering their applicability to real-world settings. This thesis introduces a multilayer microfluidic device designed for high-throughput solution exchange and efficient microparticle separation, addressing the need for processing large sample volumes at elevated flow rates. The device integrates Dean flow recirculation and selective inertial focusing of microparticles within 24 curved microchannels assembled in a compact three-layer configuration via in-plane and out-of-plane parallelization. Exploring substrate materials (glass or PDMS) and operational flow rates, we studied solution exchange and particle migration using singleplex and duplex samples across devices with varying curve numbers (2-curve, 8-curve, and 24-curve). Transitioning from glass to PDMS enhanced solution exchange efficiency in curved channels. Processing 5 μm and 10 μm microparticles at flow rates up to 16.8 mL/min (33.6 mL/min total in the multilayer device) achieved a solution exchange efficiency of 96.7%. In singleplex suspensions, 10 μm and 5 μm particles selectively migrated to different outlets of the device, demonstrating separation efficiencies of 99.7% and 90.3%, respectively. With duplex samples, sample purity was measured to be 93.4% and 98.6% for 10 μm and 5 μm particles collected from different outlets, respectively. Application of our device in biological assays was shown by performing duplex experiments where 10 μm particles were isolated from *Salmonella* bacterial suspension with purity of 97.8%. This parallelization enabled desirable combinations of high throughput, low-cost, and scalability, without compromising efficiency and purity, advancing the technology towards sample preparation.

Acknowledgments

I would like to express my heartfelt gratitude to Professor P. Rezai and Professor R. Hanson for their valuable guidance and support during my research. I am also grateful for the assistance provided by Dr. Nikdoost and Dr. Zabihihesari.

Table Of Contents

List of Tables

List Of Figures

Abbreviations

AC	Alternative Current
CFC	Circulating Fetal Cell
CTC	Circulating Tumor Cell
DC	Direct Current
DE	Dean Number
DEP	Dielectrophoresis
DI WATER	Deionized Water
DLD	Deterministic Lateral Displacement
E. COLI	*Escherichia Coli*
EDNA	Environmental Deoxyribonucleic Acid
FACS	Fluorescence-Activated Cell Sorting
HEK293	Human Kidney Cells
IDT	Interdigitated Transducer
II	Inner Inlet
IO	Inner Outlet
LB	Luria Broth
MACS	Magnetically Activated Cell Sorting
MPs	Microplastics
OI	Outer Inet
OO	Outer Outlet
PBS	Phosphate-Buffered Saline
PCR	Polymerase Chain Reaction

PDMS	Polydimethylsiloxane
PEO	Polyethylene Oxide
RBCS	Red Blood Cells
RE	Reynolds Number
RInSE	Rapid Inertial Solution Exchange
SU8	Substrate 8
TSAWS	Traveling Surface Acoustic Waves
WBCs	White Blood Cells
WHO	World Health Organization

List of Equations

CHAPTER 1

INTRODUCTION

1 Introduction to Microfluidic Particle Separation

The pivotal process of separating target cells (e.g., red and white blood cells) and particles (e.g., microplastics, bacteria) from non-target substances in complex and heterogeneous mixtures and washing them into clean buffers (also known as solution exchange) plays a vital role in sample preparation across various applications such as biomedical diagnostics [1]–[3], analytical chemistry [4], and environmental monitoring [4], [5]. This process encompasses activities like cell sorting to enhance or purify cell samples into distinct populations, particularly isolating rare target cell populations such as circulating tumor cells (CTCs) and circulating fetal cells (CFCs) from blood in biomedical applications [1], [3]. Additionally, it involves the separation of target analytes, e.g., environmental DNA (eDNA) [5], microplastics [6], [7], and bacteria [8]–[10], from inhibitors within fluidic samples and transferring them to clean and standard buffers before conducting target detection tests using polymerase chain reaction (PCR) [11], immunoassays [12], and other analytical methods in medical and environmental applications [13].

The escalating demand for water has globally intensified concerns about its quality. Numerous studies delve into threats to water resources, identifying contamination sources such as heavy

metals, bacteria, antibiotics, and microplastics [14],[15],[16],[17], all acknowledged as hazards to human health. Microplastics (MPs), one of the targeted contaminants in this thesis, are defined as small plastic particles falling within the dimensional spectrum of 1 μm to 5 mm [18]. These particles exist in a myriad of sizes, shapes, and densities [19]. They consist of polymers amalgamated with an array of chemical additives. MPs in the environment can exist in several predominant configurations: fragments, foams, films, fibers, and pellets are the most found MP shapes in the water resources [20]. MPs are considered amongst the emerging water contaminators that have destructive effects on aquatic ecosystems [17]. Numerous research projects have extensively investigated the presence of MPs in the air we breathe [21], the food we eat [22], and the water we drink [23]. Empirical evidence, as presented in a 2013 study on MP pollution in surface waters, indicates that 58% of microparticles in the Great Lakes are characterized by dimensions smaller than 1 mm [24]. Moreover, studies have demonstrated an increasing trend in the amount of MPs in samples taken from Lake Winnipeg, one of the largest freshwater resources in the world, between the years 2014 to 2016 [25].

Bacteria are another major source of water contamination. Numerous water sources have faced varying degrees of bacterial contamination. Sylwia Lew [26] studied the bacterial contamination of nine lakes on the Southern Baltic coast and the results showed that the bacterial contamination of water with many pathogens like *Escherichia coli* (*E. coli*), *Shigella*, *Citrobacter*, and *Salmonella* is affected by the water temperature and the availability of ammonia nitrogen.

Studies have demonstrated that the concentration of microparticles ranges from 10^{-3} particles/L for groundwater to over 10^{3} particles/L for surface water. According to guidelines established by the World Health Organization (WHO), the concentration of the five most prevalent substances

constituting microparticles in drinking water should not exceed the threshold of 300 µg/L to ensure adherence to water quality standards [27].

Regular water monitoring has been mandated by legislation in several locations, exemplified by California's State Bill 1422 [28]. Continuous monitoring of water contamination is imperative not just due to its detrimental effects on the health of living organisms but also because of the substantial economic losses it incurs [29].

Primarily, direct analysis of samples is seldom feasible, necessitating a series of preparatory steps to render them amenable to examination. Upon acquiring specimens through a process commonly referred to as sampling, the subsequent imperative phase involves sample preservation, a critical measure aimed at safeguarding the integrity of the sample from the moment of collection to the juncture of analysis. It is noteworthy to mention that the significance of sample preservation diminishes when employing analysis devices directly at the site of sample collection [30]. Among other preparatory measures, the quintessential steps encompass homogenization, size reduction, extraction, separation, concentration, purification, and cleanup. Notably, homogenization ensures uniformity within the sample, size reduction facilitates manageability, and extraction isolates desired components, while separation, concentration, purification, and cleanup contribute to the refinement of the sample for analytical precision. Target particles might need to be separated from untargeted particles and transferred to a clean buffer called particle washing [30].

Conventional methods for microparticle and cell separation and washing techniques can be categorized into labeled and label-free methods. Although labeled methods such as fluorescence-activated cell sorting (FACS) [31] and magnetically activated cell sorting (MACS) [32], [33] have been proven successful for separating cells, their operation relies on labeling cells with fluorescent dyes, antibodies, or other chemical tags [34]. This process is linked to extended processing times,

elevated operational expenses, and the need for skilled personnel, all contributing to challenges in achieving high efficiency [34], especially for on-site water monitoring applications.

Conventional label-free separation and washing methods using macroscale instruments include centrifugation [35], [36],[37] and mechanical filtration [38]. These methods are usually laboratory-based, time-consuming, and need sophisticated types of equipment which are costly and cannot be moved to the point-of-need (e.g., water plants, lakes, rivers). Due to the need for transportation of samples to central laboratories, the sample properties are prone to change and degradation before analysis. Moreover, these processes must be done by skilled labor. Depending on the sample ingredient and the concentration of the target analyte, multi-step centrifugation and solution exchange might be needed [39], [40] which elongates the process and makes it prone to more operator based errors. Last but not least, the high acceleration shock induced by high-speed centrifugation may damage cells and other bioparticles or lead to undesired cell agglomeration and the formation of irreversible pellets [1], [41].

Membrane-based filtering, another conventional method for particle separation, is limited by membrane pore size, and usually, the main problem with these devices is clogging [42]. Also, its application for deformable cells, e.g., red blood cells (RBCs) and some bacteria strains, is challenging as these cells may squeeze and damage when passing through the filter pores that are smaller than their size [39].

The size of particles for water monitoring, biological sample preparation, and some food industries is in the range of nano to micrometers [43],[44],[45], hindering the use of conventional sample preparation methods like centrifugation and filtration. Hence, manipulation of small particles using microfluidic devices has gained significant attention in many applications [46],[47],[48]. Microfluidic particle manipulation devices are smaller in comparison with conventional particle

separation devices. They can be automated and used at the point-of-need, so the results of separation with microfluidic devices have the potential to show more accuracy while they do not necessarily have to be run with skilled personnel [49]. Effective environmental assessment requires miniaturized equipment which are portable to be used on-site and provide real-time analysis of environmental samples [50]. Employing on-site microfluidic devices for environmental assessment serves as a pivotal strategy not only in swiftly analyzing samples but also in circumventing the potential alterations that could occur during transportation. These portable microfluidic tools offer a remarkable advantage by enabling real-time analysis at the collection point, thereby mitigating the risks associated with sample degradation or modification during transit. By conducting immediate assessments on-site, these devices ensure the preservation of sample integrity, providing more accurate and reliable data for environmental evaluations. This not only enhances the efficiency of analysis but also contributes significantly to informed decision-making in environmental monitoring and management [51].

The extensive use of microfluidic devices for particle separation has driven the evolution of various separation techniques over the past decades. These techniques can be categorized based on the source of force used for the separation of particles as active and passive techniques. Active techniques employ an external force while passive devices rely on the geometry of the microchannels and hydrodynamic forces to separate particles [49]. These techniques are reviewed in the following two sections, striving to report on their advantages and limitations, some of which will be addressed in this thesis as open research opportunities.

1.1 Active Microfluidic Particle Separation Methods

Suspended microparticles such as MPs and cells in a fluid can be pushed into predesigned locations, and hence sorted from each other, within a microfluidic environment using an external

force field. According to the source of the external field force for sorting particles, there are different types of active devices including dielectrophoretic devices that rely on an electric field, acoustophoretic devices that move microparticles with acoustic pressure waves, magnetophoretic separation devices which use a magnetic field to manipulate particles, and thermophoresis separation devices which rely upon temperature gradient-based forces [52].

1.1.1 Dielectrophoretic Particle Separation

Dielectrophoretic devices use an electric field to manipulate the movement of particles. These devices can be categorized into devices that use a direct current (DC) and those that use an alternative current (AC). When a neutral particle is located in a nonuniform electric field, it gets polarized and experiences a force named "dielectrophoresis (DEP)". This force is used to electrically control the microparticles suspended in a fluid. The application of this method is limited to the separation of particles with different dielectrophoretic responses [53]. For separating particles with similar dielectrophoretic responses, they should be labeled using polymeric nanobeads to achieve different dielectrophoretic properties [54].

In 2009, Lisen et al [55] reported a microfluidic device for active separation of beads and cells by dual frequency coupled DEP forces. Their device generates a nonuniform electric field by sidewall electrodes for lateral separation (Figure 1-1a). They applied two separate AC electric fields to the electrodes to make DEP forces for the separation of cells. The balance of these two fields determines the equilibrium position of particles (Figure 1-1b).

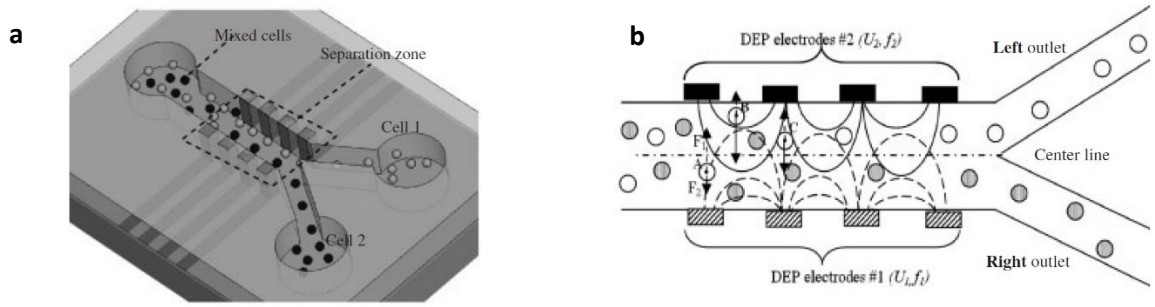

Figure 1-1 (a) Schematic view of the DEP device with two sets of electrodes on the walls at the separation zone. (b) Balance of forces on the cells at the separation zone. Reprinted with permission from John Wiley and Sons [55].

In Figure 1-1, they used polystyrene microbeads (6-15 μm), human kidney cells (HEK293), and N115 mouse neuroblastoma cells as particles for separation. Their device was able to drive 100% of beads toward bead outlet and 95% of cells toward cell outlet.

Another study conducted by Adam et al [56] used an electrophoresis microfluidic device and integrated it with a Raman spectroscopy system. They used curved electrodes combined with PDMS channels to determine the particles and map their concentration. Other studies used DEP forces by application of 3D electrodes at the top and bottom of their device [57] or fabricating electrodes from different materials including gold [58], Carbon [59], and Silicon [60].

1.1.2 Acoustophoresis

Acoustophoretic devices use acoustic waves to manipulate particle migration away or toward pressure nodes generated inside a liquid media within a microchannel. The behavior of particles in acoustophoretic fields depends on the suspending solution properties like density and compressibility as well as the particle properties like size and density [61]. In a study shown in Figure. 1-2a, Destgeer et al. [62] demonstrated a microfluidic device for sorting particles with a

cross-shaped PDMS channel design that could produce traveling surface acoustic waves (TSAWs) using an interdigitated transducer (IDT).

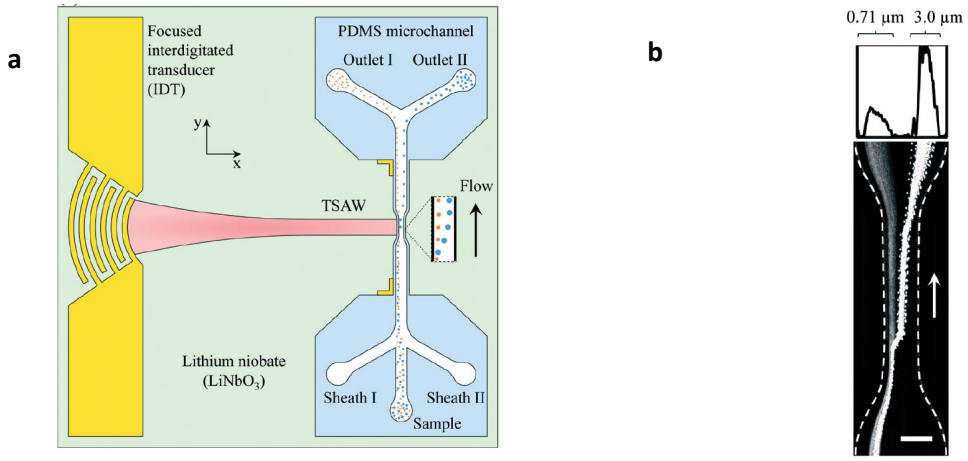

Figure 1-2 (a) Schematic view of the cross shape acoustophoretic microfluidic device for separation of particles. (b) Separated stream of 0.71 µm particles from 3.0 µm particles. Reprinted by permission from ROYAL SOCIETY OF CHEMISTRY [62].

The microchannel at the separation part in Figure. 1-2 is 200 µm wide which becomes wider near outlets to enhance separation. The channel was made in a single layer from PDMS using soft lithography and placed on top of a piezoelectric substrate ($LiNbO_3$) with the IDT deposited on it as an acoustic wave generator. The material used for IDT deposition was Au/Cr with a thickness of 1000 A, and their device was capable of separating particles with diameters of 0.71 from 3.0 µm continuously at the sample flow rate of 2.5 µL/h which were sandwiched between two sheath flows (Figure 1-2b). Other example studies have shown the application of acoustophoretic devices for focusing exosomes and separating them from extracellular vesicles [63].

1.1.3 Thermophoresis

In these devices, suspended particles are pushed toward the region with lower temperature in a media with a temperature gradient. The fundamental is similar to thermodiffusion which makes

the size of the particles critical in thermophoretic devices. Particles that can be focused in this method are usually within the range of 0.1 to 1 μm. In 2016, Ruijin [64] reported an active microfluidic device for thermophoresis sorting of sub-micrometer particles. Their device was capable of sorting particles in a range of 0.1-1 μm as an effect of the thermophoresis-induced force. Three sizes of particles were infused through the device, and they could be focused at three separate streamlines based on their size as a result of a 10k (Figure 1-3) temperature difference between the two walls. By changing the pressure difference across the channel, the position of focusing streamlines could be varied [65].

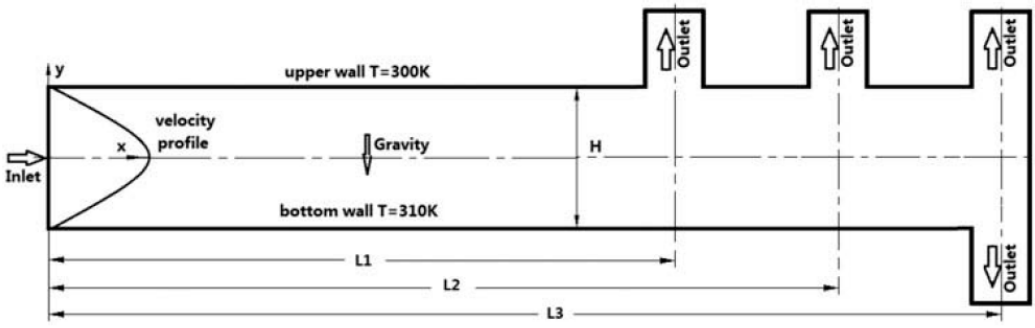

Figure 1-3 Schematic view of the active thermophoretic microfluidic device for separation of particles in three different sizes. Reprinted by permission from Taylor & Francis[64].

1.1.4 Magnetophoresis

These active microfluidic devices utilize magnetic forces to manipulate suspended particles in a medium. In 2008, Peyman et al [66] demonstrated a microfluidic device to wash particles into a new buffer using magnetic forces. Their device shown in Figure 1-4a consists of four inlets and one outlet and a reaction chamber with a width of 3mm and length of 6 mm. The device was made from glass and the depth of etched channels was 20 μm. The magnetic field was induced by a permanent magnet located on top of the device.

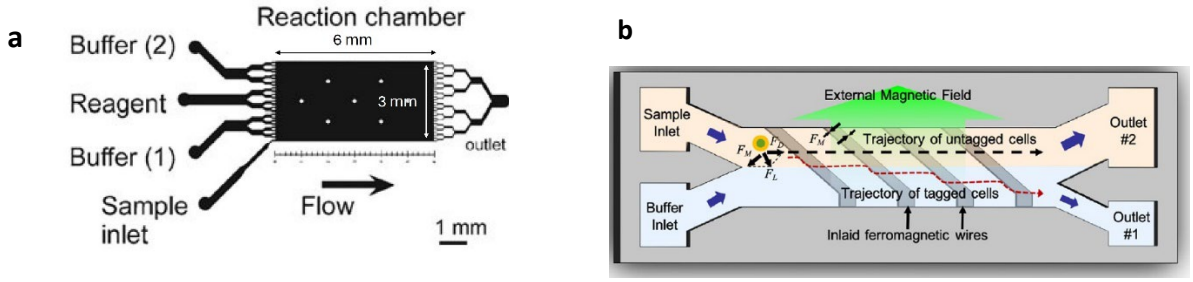

Figure 1-4 (a) A magnetophoretic microfluidic device for separation and washing of selected microorganisms. Reprinted by permission from the American Chemical Society [66]. (b) Schematic view of the microfluidic device used for active separation and washing particles to a different fluid using magnetic forces. Reprinted by permission from ROYAL SOCIETY OF CHEMISTRY [67].

Peyman et al [66] used magnetic particles with a diameter of 2.8 μm to illustrate the effect of the magnetic field and plain epoxy particles of the same size for their negative control tests. Magnetic particles were attracted by the magnetic field and pushed into the new buffer. Their device was able to process a flow rate of 1.8 μL/min and the concentration of the infused sample was 6.7×10^6 particles per milliliter. In a recent study, another magnetophoretic microfluidic device was used to isolate microorganisms that bind gold-coated beads [67]. They developed a microfluidic device that can separate microorganisms which are bound to magnetic beads and wash them into another fluid (Figure. 1-4b), reaching a separation efficiency of 70% at a flow rate of 0.033 mL/min.

All in all, active particle manipulation devices exhibit the capability to adeptly reorganize particle positions and exercise precise control over particle displacement. Nevertheless, the construction of active microfluidic devices typically necessitates the incorporation of metallic components such as electrodes or elements inducing magnetic fields. This inclusion imparts a degree of complexity and expense to the fabrication process. In the realm of active devices, residual time is requisite to facilitate the application of external forces for particle manipulation. This temporal consideration assumes a pivotal role as a constraining parameter, particularly under conditions of low flow rates [52].

The demand for particle manipulation devices featuring elevated flow rates, coupled with a simplified structural design, is conspicuous. This imperative can be effectively addressed through the utilization of passive particle separation devices.

1.2 Passive Microfluidic Particle Separation Methods

As opposed to active separation devices, passive devices do not utilize any external force fields to manipulate particles. They rely entirely on hydrodynamic fluid flow forces and the channel design and geometry. Passive methods include Deterministic Lateral Displacement (DLD), viscoelastic microfluidics, and inertial microfluidics but are not limited to them.

1.2.1 Deterministic Lateral Displacement (DLD)

These devices, as schematically shown in Figure. 1-5, use a specific array of pillars to produce a peerless flow streamline to manipulate particles based on their size. Using this method, particles smaller than a critical size move forward with the flow while large particles move laterally in a zig-zap path through the pillars [61]. In 2004, Huang et al [68] reported a microfluidic device for the passive separation of particles using the DLD method. Their device was capable of continuously focusing 0.8, 0.9, and 1.0 µm particles with a resolution of 10 nanometers at a flow speed of 400 µm/s. They demonstrated that particles follow two transport modes based on their size. In another study, Brian [69] reported a DLD microfluidic device for the separation of circulating tumor cells (CTC) with a diameter of 10-15 µm from red blood cells sized 6-8 µm at a relatively high Reynolds number ($10 < Re < 60$). Other studies show the application of a dielectrophoretic DLD technique to detect CTC in the blood [70]. Their device combines size-based and dielectric properties of particle separation (Figure 1-5). They demonstrated separation

of CTCs from WBCs using this device that had two inlets and two outlets, one of the inlets was designed for the sample and the second for the running buffer. One of the outlets collects CTCs and the other outlet is placed to collect the rest of the sample.

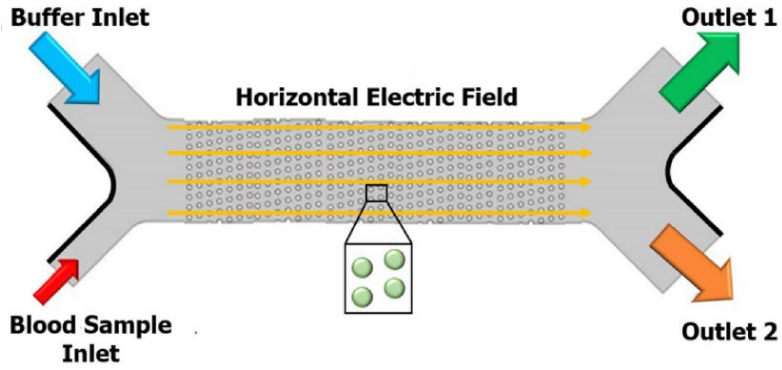

Figure 1-5 Structure of a microfluidic device using combined effect of dielectrophoretic with a horizontal electric field and DLD method for separation of CTCs from blood cells. The horizontal electric field generated by applying AC electric potential to the V-shape boundaries shown as thick lines. Outlet 2 is designed to collect the separated CTCs and Outlet 1 is placed to collect the rest of sample. Reprinted by permission from Springer Nature [70].

The results show that the dielectrophoretic DLD can separate CTCs from WBCs continuously by applying an electric field with a frequency near CTCs`s crossover frequency. This combination of a passive and active method can separate cells even with overlapping sizes based on their dielectric properties with a maximum flow rate of 40 µL/min.

1.2.2 Inertial Microfluidics in Straight Microchannels

In inertial microfluidics, the dominant forces applied to microparticles are inertial forces including the wall-induced lift force and the shear gradient lift force. Reynolds number is defined as the ratio of inertial forces to viscous forces ($Re = \frac{\rho UD}{\mu}$ where ρ, U, D, and μ are fluid density, fluid velocity, hydraulic diameter, and dynamic viscosity, respectively). In traditional microfluidics, inertia is negligible due to the low Reynolds number (Re<1), however, in inertial microfluidics, Reynolds

number is in an intermediate range (~1<Re<~100) which is more than Stokes flow but still less than turbulence flow. Particles moving in a fluid in a microchannel are under the effect of several forces including viscous drag force (F_{drag}) due to the movement of particles through a fluid, Magnus force due to the rotation-induced lift force, Saffman force due to slip-shear induced lift force, wall induced lift force (F_{LW}) due to the flow field changes around a particle near channel walls, and shear gradient lift force (F_{LS}) as a result of the parabolic velocity profile that is scalable with respect to the particle size in a channel. For a spherical microparticle in a straight microchannel, Magnus and Saffman forces are negligible while the shear gradient lift force drives the particles toward the channel walls and wall-induced lift force pushes the particles to the channel centerline.

Wall-induced lift force (F_{LW}) is an effect of the change of flow field around a particle near the wall regions. Walls decelerate the particles and lead to a slightly lower velocity of particles than the fluid and also cause a pressure that pushes the particles away toward the channel centerline (Figure 1-6). This force reduces when the distance of the particles increases from the channel walls. The magnitude of wall-induced lift force can be calculated by equation 1-1 [71].

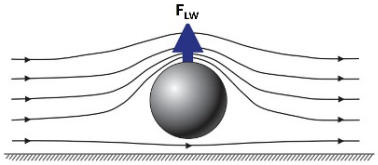

Figure 1-6 Wall-induced lift force (F_{LW}), pushes the particles away from the wall. Reprinted by permission from ANNUAL REVIEWS [71].

$$F_{Lw} = \rho U_{max}^2 C_w a^6 / D^4 \quad (1\text{-}1)$$

In this equation, ρ is the fluid density, U_{max} is the maximum fluid velocity, C_w is the wall lift coefficient which is a function of Reynold number and particle lateral position, a is the particle diameter, and D represents the hydraulic diameter of the channel (4×Cross section/Perimeter).

Shear gradient lift force (F_{LS}) arises as a reason of different relative velocities at the two end sides of the particle (Figure. 1-7). The velocity profile in a microchannel is parabolic and the relative velocity at each side of the particle is different which results in a force toward the side with higher relative velocity (i.e., lower pressure). As such, the direction of the shear gradient lift force is toward the channel walls when particles are closer to the channel centerline.

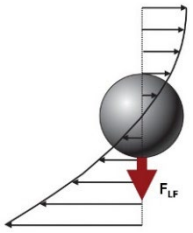

Figure 1-7 The Shear Gradient Lift Force (F_{LS}) arises as a reason of different relative velocities at the two end of the particle and drives particles toward channel walls. Reprinted by permission from ANNUAL µREVIEWS [71].

The magnitude of the shear gradient lift force like wall-induced lift force is a function of fluid density (ρ), the maximum fluid velocity (U_{max}), shear gradient lift force coefficient (C_s), size of particle (a) and the channel hydraulic diameter (D) and can be calculated through equation 1-2.

$$F_{LS} = \rho U_{max}^2 C_s a^3 / D \quad (1\text{-}2)$$

The net inertial lift force from the two above forces that a particle experiences in a microchannel can be calculated using equation 1-3. A balance between the wall-induced lift force and the shear gradient lift force determines the equilibrium position of the particles between the channel

centerline and the channel walls in inertial microfluidic devices [72]. In a straight microchannel, this equilibrium position is close to the centerline of the longer channel cross-sectional side, and 0.2-width away from the channel wall. It must be noted that for the particles to focus, a/D ratio should be larger than 0.07 and the particle-based Reynold number ($Re_P = Re\ (a\ /\ D)^2$) must be larger than unity [73].

$$F_L = f_L \rho_f U^2 a^4 / D^2 \tag{1-3}$$

Where f_L, ρ_f, $U, a\ and\ D$ are the lift coefficient, fluid density, diameter of particle, and channel hydraulic diameter respectively. The lift coefficient is a function of Reynold number and particle lateral position. For Re<100 which is in the range of inertial microfluidics, the lift coefficient can be estimated as f_L=0.5 [74].

In a straight channel for particles at the equilibrium position, the net inertial lift force is balanced with the Stokes viscous drag force in equation 1-4 which arises as a result of lateral movement of the particles with a lateral velocity of U_L before arriving at the equilibrium position. In this equation a and μ represent the diameter of particle and the dynamic viscosity of fluid respectively.

$$F_{stks} = 3\pi\mu a U_L \tag{1-4}$$

The straight channels are the simplest inertial microfluidic devices for the manipulation of microparticles, Hue $et\ al$ [75] reported a microfluidic device for inertial enrichment of adrenal cortical cells using a straight microchannel length of 4.5 cm, an expanding region, one inlet, and three outlets (Figure. 1-8). They used conventional PDMS soft lithography to make the device and processed 5 mL of cell solution with a throughput of 24,000 cells/min with a flow rate of 60 µl/min. As demonstrated, large cell clumps were inertially focused at the center of the channel and enriched while the small cells did not experience inertial focusing and were extracted from the side outlets.

Results showed the purification of adrenal cortical progenitor cells with a viability rate near the main cell solution in which more than 70% of collected cells remained viable.

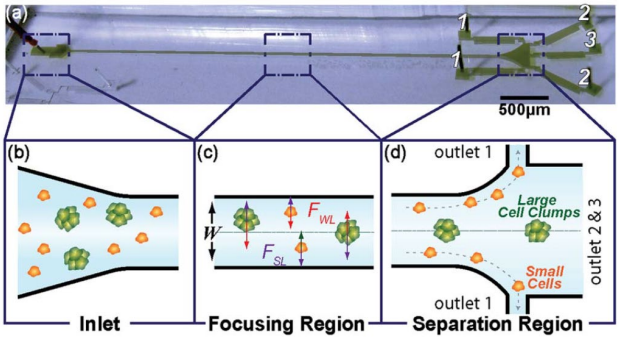

Figure 1-8 Microfluidic device with one inlet, two side outlets and a center outlet for size-based separation of particles using inertial forces in a straight microchannel [75].

Extracting particles from the original solution and washing them into a clean buffer is widely used in sample preparation or post-treatment of processed samples. For example, in order to process biological samples, particles should be moved to an antimicrobial buffer. Another use of particle washing is moving microparticles from the contaminated sample to a clean buffer. Researchers have done several studies on particle washing and solution exchange using inertial microfluidics. Daniel R. Gossett et al [76] introduced a passive microfluidic device for rapid inertial solution exchange (RInSE) of cells and putting or moving them from a reaction buffer. Their device consists of two parts: the first is a particle-focusing device, and the second is designed to migrate focused particles to a clean buffer (Figure. 1-9). They used a co-flow of sample solution and the clean buffer in a straight channel, the device was capable of processing 60 µl/min of sample to a clean buffer with a flow rate of 90 µl/min. They collected 97% of 20 µm entering particles at the predicted outlet and the purity of the collected buffer was 100%.

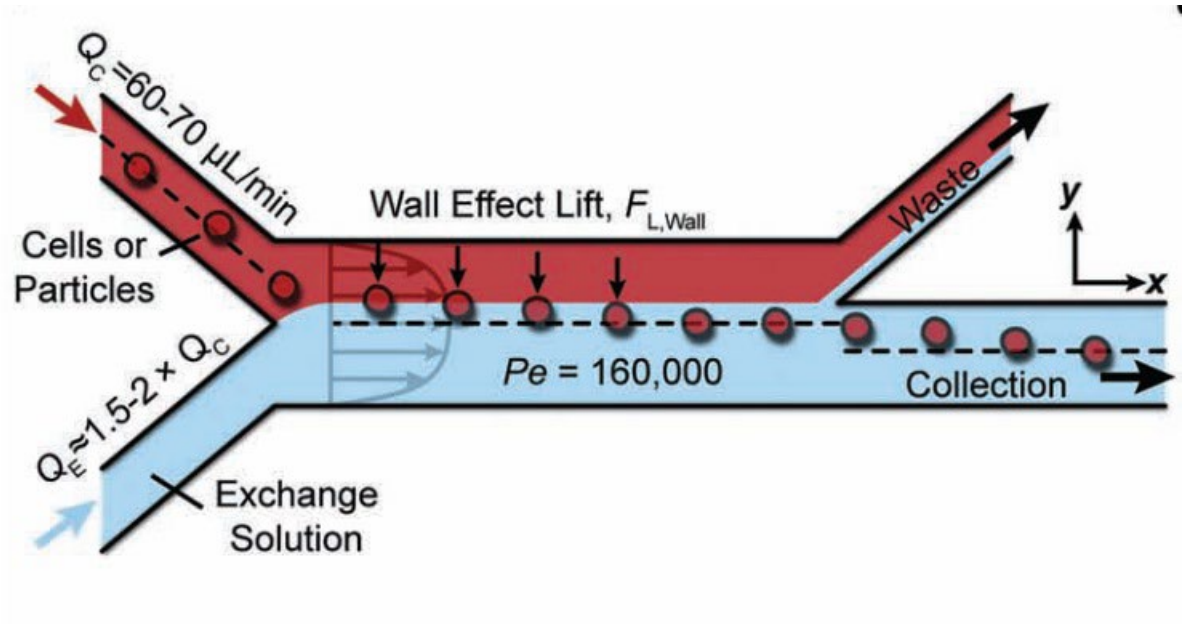

Figure 1-9 Schematic view of microfluidic device using inertial forces for solution exchange of particles with diameter of 10 µm into a coflowing solution. Reprinted by permission from John Wiley and Sons [76].

Jaideep [77] reported a straight microchannel device for rapid inertial solution exchange (RInSE). The device consists of a straight microchannel with three inlets and three outlets. At the inlets, sample solution was infused from the side inlets and the clean buffer was injected through the middle inlet (Figure 1-10). These three solutions formed a laminar co-flow with negligible diffusion. The wall induced lift inertial forces drove pre-focused particles from the main solution into another solution stream in the middle of the channel within milliseconds. At the outlet, the target particles exited through the middle outlet within the clean buffer and two side outlets were used to collect the waste solution.

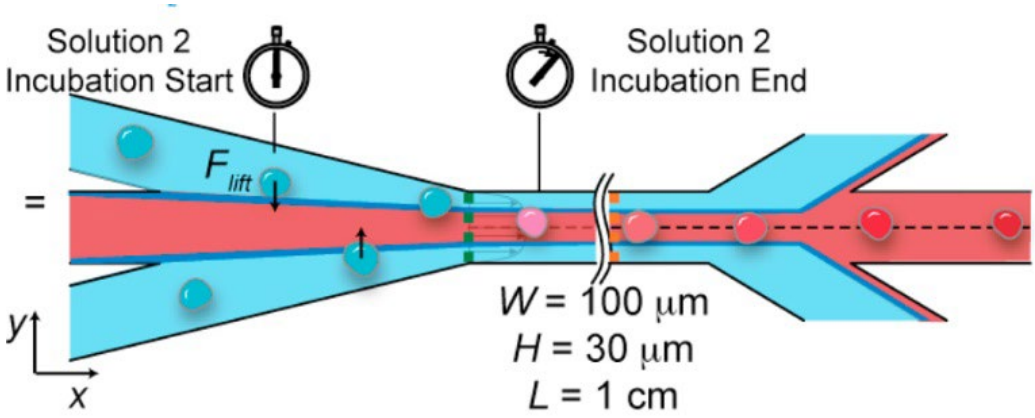

Figure 1-10 Inertial Microfluidic device for solution exchange of particles (a=19 µm) and cells (a=15 µm), main sample enters the channel from side inlets (Q= 30 µL/min) and the target solution is injected from the middle inlet (Q=100 µL/min). Reprinted by permission from American Chemical Society[77].

They reported a separation efficiency of 100% for 19 µm polystyrene beads and 81.5% for cells with a diameter of 15 µm at the sample and target solution flow rates of 30 µL/min and 100 µL/min, respectively. The purity of the final solution was 98.5% and they collected 81.4% (recovery rate) of the infused cells in the outlet solution. In another study, Zhou et al [78] reported an inertial microfluidic device for focusing particles in two stages. Their device had a purity of 99% and they reached the operational flow rate of 100 µl/min.

Fabrication of straight channels is easy and their operation is simple. However, the cross-section of these microchannels is confined since the lift force (F_L) is related to the reverse square of the channel hydraulic diameter ($F_L \propto D^{-2}$) [79]. In addition, straight channels should be long enough for migrating the particles to their equilibrium positions (L_{min}), which would lead to high hydraulic resistances. Flow rate and processing throughput is limited in straight microchannels, and yet another challenge associated with straight microchannels is that particles mostly focus on 2-4 equilibrium positions which makes their separation and solution exchange further complicated, as opposed to a desired state of equilibrium with one position in the channel that is easier to work with.

1.2.3 Inertial Microfluidic in Curved Microchannel

As opposed to a streamlined laminar primary flow in a straight microchannel, a secondary lateral flow regime emerges in curved microchannels (Figure. 1-11) as a result of the mismatch of velocity between the fluid elements near channel walls and in the centerline of the curved microchannel. The inertia of fluid elements around the centerline is greater than near the walls which results in their outward movement. This flow creates a pressure gradient resulting in two counter-rotating cross-sectional vortices in the lateral direction called Dean flow. Although the flow mechanism of the curved microchannel is more complicated than a straight channel, the Dean flow will alter and sometimes enhance the inertial migration of particles besides providing modified equilibrium positions [79]. This is mainly because the Dean flow will apply a lateral drag force to particles which makes some of the inertial equilibrium positions of the particles unstable, sometimes reducing the states of equilibrium to only one position with zero net force balance. In addition to curved microchannels, flows around micropillars in a microchannel and inside serpentine and expansion-contraction channel geometries can also create a secondary flow similar to the curved channels [49].

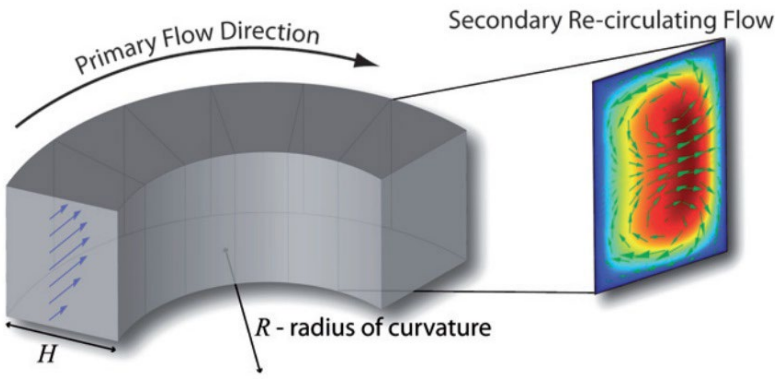

Figure 1-11 Formation of Dean flow in curvilinear microchannel. The higher velocity near center line extends outward. As a result of conservation of mass stagnated fluid near walls move inward. This flow makes two vortices in a perpendicular direction to the main flow. Reprinted by permission from ROYAL SOCIETY OF CHEMISTRY. [80]

Many researchers have taken advantage of these circulating flows in their microfluidic devices for precise manipulation of particles and fluids movement in curved microchannels. Dean flow has been applied for various sample preparation processes such as continuous separation of CTC [81], [82], fluid mixing [83],[84] solution exchange [85],[5],[8] and filtration [86].

In curved microchannels the velocity of fluid elements at the centerline does not match the velocity near the walls. This causes the fluid element with larger inertia to move from the centerline toward the outer wall. This movement of fluid elements creates a radial pressure gradient and stationary fluid elements near the channel wall move inward due to this pressure gradient. This circulating movement of fluid creates two counter-rotating vortices which are called Dean vortices (Figure. 1-11). The strength of this flow is determined by a dimensionless number called Dean number in equation 1-5, in which R, D, and Re are the channel radius of curvature, channel hydraulic diameter, and Reynolds number, respectively. [87].

$$De = \sqrt{\frac{D}{2R}}\,\mathrm{Re} \tag{1-5}$$

When particles circulate with these vortices, a small drag force arises, as the lateral Re number is small ($Re_L < 0.2$). This drag force can be calculated by the Stokes drag formula (equation 1-4), where U_L has to be replaced by the average velocity of the fluid vortices, called the Dean velocity (V_{De}). In 2004, Ookawara [88] reported an experimental equation for the average Dean velocity which relied only on Dean number. In 2017, Bayat et al [89] reported an improved semi-empirical estimation of average Dean velocity (equation 1-6), where the effect of channel geometry and viscosity were accounted.

$$V_{De} = 0.031 \left(\frac{\nu}{S}\right) De^{1.63} \tag{1-6}$$

In this correlation, ν represents the fluid kinematic viscosity (μ/ρ), S is the channel largest cross-sectional dimension, and De is the Dean Number. The ratio of the net inertial force (equation 1-3) to the Dean drag force (equation 1-4 using V_{De} from equation 1-6), as shown in equation 1-7, has been reported useful to identify whether inertial focusing happens in curved microchannels or not [90].

$$R_f = \frac{F_L}{F_D} = \frac{f_L \rho U^2 a^3}{3\pi\mu D^2 V_{De}} \tag{1-7}$$

In this equation f_L represents the lift coefficient, ρ denotes the fluid density, U signifies the axial velocity, and a stands for the particle diameter. D, $V_{De,}$, and μ correspond to the channel hydraulic diameter, average Dean velocity, and dynamic viscosity of the fluid, respectively.

As an estimation, $R_f \gg 1$ indicates the dominance of net inertial left force in which inertial focusing will happen, while $R_f \ll 1$ can be known as the dominance of the Dean drag force which shows that particles will recirculate by the Dean vortices and do not focus [90].

Many studies have been conducted on the manipulation of particles using Dean flow in curved microchannels. Niveditaa [91] reported a spiral microchannel for continuous focusing and separation of particles based on their size. In another study, Wirttick [92] demonstrated a spiral microfluidic device for the separation of Circulating Tumor Cells (CTCs) with a purity near 100% and throughput of 2.47mL/min. Other geometries have been designed for inertial particle separation including serpentine [93] and expansion-contraction designs [94].

In 2018, in our group, Bayat et al [8] made a curved microchannel for washing target particles and separating them from bacteria. Their device consists of a curved channel with two inlets and two outlets (Figure 1-12). Sample was always injected into the device from the inner-wall inlet along with a clean buffer solution that was co-injected from the outer wall inlet. In their device, bacteria moved from the inner wall toward the outer wall as a result of dominant Dean flow induced lateral drag forces ($R_f \ll 1$, Figure 1-12A). On the contrary, larger particles were dominated by inertial lift forces ($R_f \gg 1$) and focused near the inner wall of the curved microchannel (Figure 1-12B). Moreover, the effect of various device and flow parameters on the Dean flow was investigated in order to achieve a complete fluidic position switching (180-degree Dean recirculation), for instance from the inner-wall inlet to the outer-wall outlet of the device. This enabled the larger particles to not only be focused, but also be washed from the original sample into the clean buffer simultaneously (Figure 1-12B).

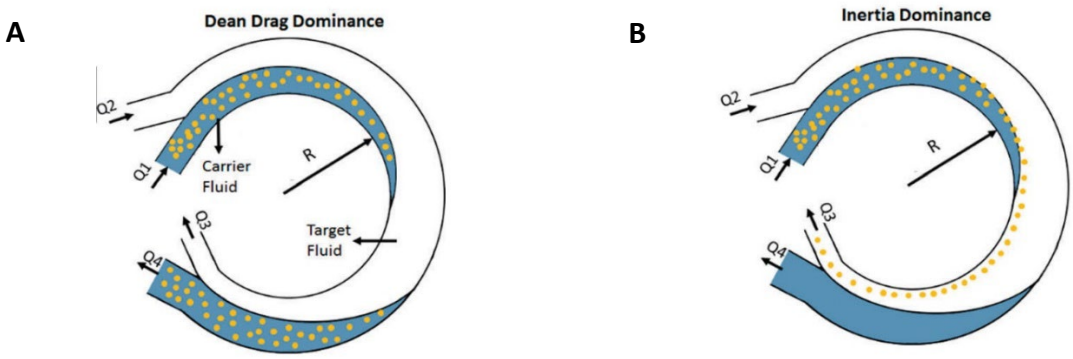

Figure 1-12 A centrifuge inertial microfluidic device for particle manipulation and washing. A) Smaller particles like bacteria are dominated by the Dean drag force and circulate within the secondary flow. B) Larger particles are dominated by the inertial forces and focus near the channel`s inner wall. Reprinted with permission from ROYAL SOCIETY OF CHEMISTRY [8]

The device in Figure 1-12 which became the bases of research work in this thesis was able to process particles at a flow rate of 1 mL/min with a throughput of 10^4 particles per milliliter. They reported solution exchange of 19 µm particles with the efficiency of 93±0.7% for single particle size. In a duplex experiment for separation of 11 µm from 4 µm particles the achieved purity was 96±2%.

One of the confining aspects of the above reviewed microfluidic devices is their low flow rates, especially when it comes to industrial and environmental applications, or for processing samples with rare particles that there is a need to process a large volume of samples. Many researchers have tried to increase the flow rate in microfluidic devices with various methods. One of the used methods for increasing the flow rate is modifying the channel cross-section. Guofeng et al [95] reported a spiral microchannel with a trapezoidal cross-section, and results showed an increase in the strength of dean vortices which enabled higher flow-rate for particle separation. Other studies have also been conducted on the effect of cross-section shape on inertial forces to reach higher flow rates [96][97].

In-plane arraying or parallelization of multiple devices is another approach to increase the flow rate of sample processing in inertial microfluidic devices. Mach [98] introduced a microfluidic device for the filtration of blood at high flow rate in which their device consisted of 40 microfluidic devices connected to each other in a polar array, while each device was formed from a straight channel with one inlet for injecting sample, a focusing channel, an expansion region, and three outlets (Figure. 1-13a). Their device was capable of removing more than 80% of bacteria from diluted blood after two passing of the device. By this massive in-plane parallelization, they reached the flow rate of 4 mL/min and a high throughput of 400 million cells per minute. Other studies have also been done for in-plane parallelization of devices [93].

Out-of-plane device parallelization and a combination of in-plane and out-of-plane methods, are other approaches for increasing the device flow rate. In 2015, Warkiani et al [99] demonstrated a multi-layer device with four parallelized spiral channels (Figure 1-13b) in each layer for microfiltration and separation of particles. The device works in two modes of fractionation or filtration. In fractionation mode larger particles focus near the inner wall while smaller particles migrate toward the outer wall of spiral channels. In the fractionation mode the flowrate per spiral device is 2 mL/min (total flowrate of 80 mL/min for the 10-layer device with 4 interconnected spiral channels in each layer). In the filtration mode all the particles are focused near the outer wall as a result of dominance of the Dean drag forces. The optimum flowrate for the filtration is 6 mL/min per each spiral device (total flowrate of 240 mL/min for the 10-layer device including 4 parallelized spiral channels in each layer). Their team in 2016 [100] made a parallelized slanted spiral microchannel device for separation of blood plasma and gained a flowrate of 24 mL/min for processing diluted blood samples. Other studies have also been conducted for increasing flowrate in multi-layer devices [96].

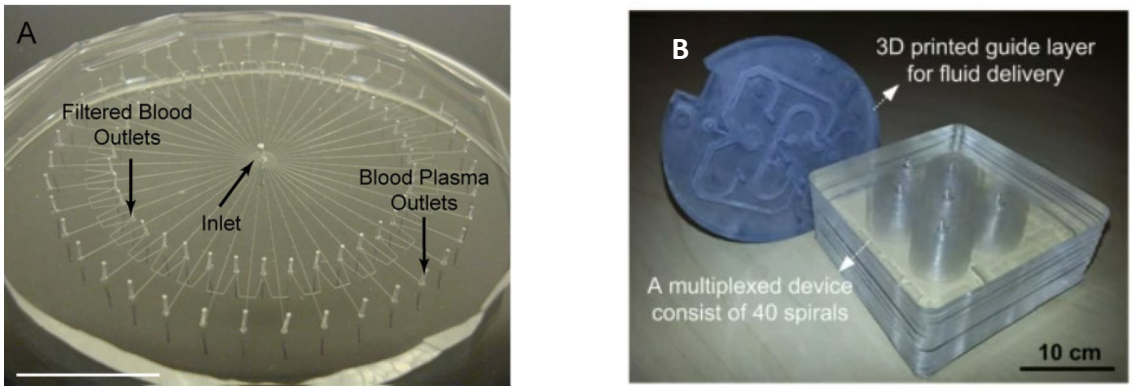

Figure 1-13 Parallelization of microdevices for increasing the flowrate of the device. A) In-plane parallelization of 40 straight channels for inertial filtration of blood. Reprinted with permission from John Wiley and Sons [98]. B) Combination of In-Plane and out of plane parallelization of spiral microchannels for separation of Chinese Hamster Ovary (CHO) cells from yeast at high flowrates. Reprinted with permission from Springer Nature [99].

In a recent study in 2022, Fang [1] introduced a multi-layer centrifuge microfluidic device for extracting bacteria and washing CTCs to a clean buffer. They used four parallelized spiral microchannels for extracting and washing target particles in the range of 10-20µm and two serpentine microchannels for increasing concentration of target particles in the buffer (Figure. 1-14). The device consisted of five microfluidic layers and four adhesion layers. Channel layers were made using polymer films and UV laser cutting, then enclosed by bonding to adhesive layers. The device was capable of processing samples with a flow rate of 400 µL/min per each spiral channel and wash them to a buffer, at a total flow rate of 2.4 mL/min and with a recovery rate of over 93%.

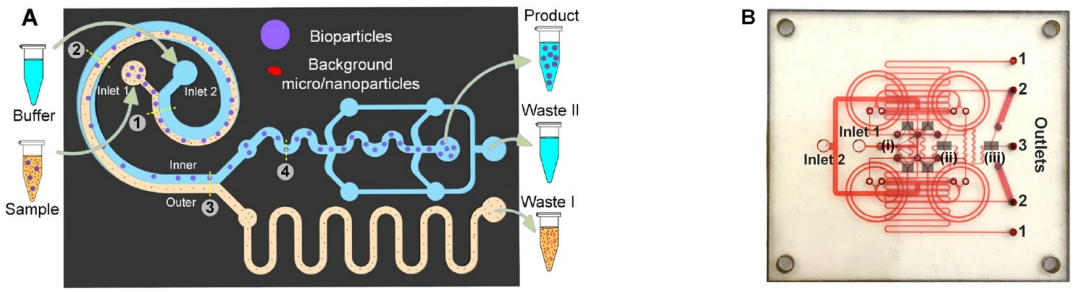

Figure 1-14 A miniaturized centrifuge device for washing and concentrating particles A) schematic diagram of device consisting of a spiral channel with two inlets for washing particles and a serpentine microchannel for concentrating the target particles. B) Photograph of the miniaturized device with five channel layer and four adhesion layers. Reprinted with permission from ROYAL SOCIETY OF CHEMISTRY [101].

1.2.4 Viscoelastic Microfluidics

The fluidic phase in many multi-phase samples is not aqueous with examples including the blood, saliva and raw milk. The continuous phase in these samples can show viscoelastic, shear thinning, or shear thickening effects. The area of viscoelastic microfluidics mostly refers to the investigation of viscoelastic fluids like Polyethylene oxide (PEO)-spiked water samples with suspended particles in microfluidic channels. In viscoelastic separation microfluidic devices, particles migrate to the equilibrium positions as a result of a balance between three dominant forces including inertial lift forces (F_L), elastic forces (F_E) and viscous drag force (F_D) [102]. Researchers have reported devices for separation of particles and solution exchange in viscoelastic fluids [103],[104]. In 2023, Nikdoost et al. [105] combined the effect of inertial lift, elastic, viscous drag and Dean drag forces to fabricate a curved-channel microfluidic device for focusing of particles in PEO water solutions. We restrained from providing a thorough review on viscoelastic microfluidics as this thesis mainly focuses on particle suspensions in water.

1.3 Technological and Scientific Knowledge Gaps

Fabricating passive microfluidic devices is simple and they are cheaper to make, but they are limited in terms of flow rate as discussed in the previous sections. In many industrial and environmental applications like water monitoring, there is a need to process a considerable volume of sample (10s of mL to few L) in a reasonably short time (less than 1hr) and with high separation and washing efficiencies and purities. In many cases like biological sample preparation, target particles are rare in the solution, emphasizing the importance of achieving a high recovery rate in sample preparation. Although some research has been conducted to increase the flow rate of microfluidic devices, there is still an unmet need for simultaneous size-based separation of small particles from other particles or bacteria, and washing them to a clean buffer at a high flow rate and with high separation efficiency and solution exchange purity. Here, we employed an innovative approach involving both in-plane and out-of-plane device parallelization to augment the flow rate of our curved microfluidic device for concurrent particle-particle and particle-bacteria separation and simultaneous solution exchange.

1.4 Objectives of the Thesis

According to the literature studies, most of the research has been focused only on separating of particles or driving particles from a solution to a buffer separately but fewer studies have been done on simultaneous separation and washing particles in a single microfluidic device at high flow rates. In this thesis, we aimed for a size-based separation of particles in a curvilinear microchannel by applying a combined effect of inertial and Dean drag forces, while using a co-flow inlet and outlet structure to simultaneously wash the separated particles into a clean buffer at high

throughput ($\sim 10^5\ particle\ per\ mL$), and at a high flowrate (>15 mL/min). To approach our goals, we followed these objectives:

Objective 1: Designing a curved microchannel for particle focusing/washing and parallelizing it in polar and rectangular arrays in one layer and comparison between these two arraying methods.

Objective 2: Out-of-plane parallelization and stacking of the curved microchannel design with the best array to enhance the throughput of the device.

Objective 3: Testing the performance of the parallelized device with a water sample containing *Salmonella* bacteria and microparticles to assess its separation and washing characteristics.

1.5 Chapter Organization

In Chapter 2, we have discussed the fundamentals of designing the channel with proper size and geometry to achieve particle separation and solution exchange at the outlet of the device following with the materials and methods used in this thesis. In Chapter 3, we have addressed the first objective of the thesis by parallelizing the designed device in a stepwise manner by doubling the number of the curve channels at each step and in two distinct patterns of polar and rectangular arrays. We used co-flow fluids with distinct colors to analyze the solution exchange in each design and choose the best array method for the next objective. In Chapter 4, focusing on objective 2, we have reported the effect of the material of the base substrate on the solution exchange and developed a multi-layer parallelized device for sized-based separation of particles and washing the target particles into a clean buffer. We also tested our device with a solution of duplex size particles in a dyed solution to study the simultaneous separation and washing of target particles. Finally, we tested the device with a biological sample to investigate the application of the device in water

processing as proposed in objective 3. Lastly, in Chapter 5, the main achievements of the thesis have been summarized and opportunities for future research have been discussed.

CHAPTER 2

MATERIALS AND METHODS

2 Materials and Methods

2.1 Microparticle and Bacteria Spiked Water Samples

As discussed in section 1.4, in objectives 1 and 2 of the thesis, we solely used DI water samples spiked with various microparticles for curved-channel microfluidic device development and optimization. We then shifted towards working with *Salmonella* bacteria and microparticles spiked in water to achieve objective 3 of this thesis.

Particle-free water behavior investigations were conducted first to examine the solution exchange behavior of the parallelized curved-channel microfluidic devices. This was performed using a co-flow of undyed and dyed DI water into the devices, where 15% v/v trypan blue (Sigma Aldrich, USA) was used to dye one of the fluid streams inside the microchannels.

Bacteria samples of *Salmonella* (Carolina® Biological Supply Company, Burlington, NC, USA) were picked from a single colony on a source agar growth plate and cultured overnight in Luria Broth (LB) on a shaker incubator at 37℃ and 200 rpm. The cultured bacterial suspension

underwent serial dilution and standard plate culturing was used to quantify the bacterial concentration in the source and the diluted levels.

Microparticles used were 4.7 µm (~ 5 µm, CM-50-10, 2.5 %w/v) and 10.4 µm (~ 10 µm, CM-100-10, 1% w/v) in size and procured from Spherotec Inc. These microparticles were spiked into DI water at the concentration of 10^5 particles per millilitre to prepare the particle solutions. Tween 20 (Sigma Aldrich, USA) was added to the particles' solutions with a concentration of 1% v/v to prevent particle aggregation.

For the generation of 5µm particle solutions at a concentration of 10^5 particles/mL, 16.7 µL of the commercially acquired particle solution (concentration: 6×10^8 particles/mL) was introduced into 100 mL of DI water. The methodology employed for the production of the 10 µm particle solutions was identical, with 549 µL of the procured particle solution (concentration: 1.819×10^7 particles/mL) being mixed with 100 mL of DI water. Duplex particle investigations were performed with a total particle concentration of 10^5 particles/mL as well. In the creation of a duplex-sized particle solution, the quantity of the primary particle solution was halved compared to the aforementioned volumes. This adjustment was made to sustain a consistent concentration of total particles at 10^5 particles/mL.

For the mixed suspension of *Salmonella* bacteria and microparticles, 5 µm and 10 µm microparticles were spiked into the *Salmonella* bacteria solution to make concentrations of 10^5 particles/mL for microparticles and 10^5 CFU/mL for *Salmonella* bacteria. The mixture of *Salmonella* and particles was used as the carrier fluid suspension, while phosphate-buffered saline (1% PBS) was used as the washing fluid in all bacteria-based experiments.

2.2 Curved Microfluidic Channel Design

The initial design of our curved channel microfluidic device was similar to the one shown in Figure 1-12 with two inlets, one curved microchannel, and two outlets. However, the total length of the microchannel had to be reduced approximately to half a circle (180 degrees angle) so that the device could be replicated in parallel designs for throughput enhancement as aimed in this thesis. Our criteria for the water-suspended particles and *Salmonella* bacteria in these devices were 1) for the larger particles to focus at the inner wall outlet of the curved microchannel (and hence get washed into the clean buffer), and 2) for the smaller particles, or the bacteria, to be carried out in the original sample and from the outer wall outlet of the device.

To design a curved microchannel for size-based separation of microparticles and their simultaneous solution exchange, we need to have a clear understanding of the physics of Dean vortices and the dominant forces acting on the particles in the flow. As there is still not an analytical solution for Navier-Stokes equations for a fluid flow through a curved microchannel, we used the semi-empirical equation of average Dean velocity (V_{De}) reported by Bayat et al. in 2017 [89] (equation 1-6). This equation can help us predict Dean fluid flow recirculation and switching in a curved microchannel. Our objective was to obtain a full switch in the position of the sample and clean buffer streams inserted into the curved microchannel from the inner and outer wall inlets, respectively (as shown in Figure 1-12).

To design our device for particle focusing, we investigated the net inertial lift force and the drag force on 10 and 5 µm particles and the ratio of lift to drag force (R_f in equation 1-7). The optimized design should have had the largest possible R_f for the bigger particles to focus at the inner wall and the smallest possible R_f for the 5µm particles to be carried in the Dean flow. Moreover, it should be reminded that the ratio of particle diameter (a_p) to channel hydraulic diameter (D_h) must be

more than 0.07 to enable particle focusing to their equilibrium positions [106]. Simultaneously, to maximize the purity of the clean buffer at the inner outlet, the length (L) and the radius (R) of the microchannel had to be correctly designed to obtain only one switch of the fluid positions in the curved channel.

More than 3500 possible curved microchannel geometries were theoretically investigated in this thesis, with some examples related to one of the channel designs shown in Table 2-1. In this study, channels characterized by varying dimensions in terms of height (h), width (w), and R were systematically examined. For each specific channel geometry, key parameters such as hydraulic diameter (D_h), Reynolds number (Re), Dean number (De), and average Dean velocity (V_{De}) were computed using the equations provided in Chapter 1. The outcomes of these computations were subsequently employed to determine the ratio of lift to drag forces, $R_{f\text{-}5}$ and $R_{f\text{-}10}$, for particles with diameters of 5 μm and 10 μm, respectively. Our objective was to identify the conditions (channel design and volumetric fluid flow rate Q) that could provide the most distinctive R_f values for these two particle sizes within the spectrum of feasible channel designs. At the same time, we had to make sure that the two fluids perform a single switch by the time they exit from the outlet (i.e., desired fluids switching angle = 180 degrees). For calculating the switching angle, we utilized the method provided by Bayat et al. [89]. In this method, V_{De} calculated from equation 1-6 is used to determine the length of the channel at which the fluids perform a lateral displacement equivalent to the half of the channel width (L_{switch}). This length is easily converted into the switching angle using the channel radius of curvature.

Table 2-1 An example of calculations conducted in this thesis for designing curved microchannels. The key parameters were calculated at a constant total flow rate of 2 mL/min in a single curved channel device with w=300µm width and h=70µm height (D_h=113.5 µm)

R (mm)	V_{De}(mm/s)	R_{F-5}	R_{F-10}	Switching Angle (degree)
5	1.27	0.23	1.83	210.32
6	1.10	0.27	2.13	203.35
7	0.97	0.30	2.41	197.63
8	0.87	0.34	2.69	192.81
9	0.79	0.37	2.96	188.65
10	0.72	0.40	3.22	185.01
11	0.67	0.44	3.48	181.78
12	0.62	0.47	3.74	178.87
13	0.58	0.50	3.99	176.24
14	0.55	0.53	4.24	173.84
15	0.52	0.56	4.49	171.64
16	0.49	0.59	4.73	169.60
17	0.47	0.62	4.97	167.71
18	0.45	0.65	5.20	165.95
19	0.43	0.68	5.44	164.29
20	0.41	0.71	5.67	162.74
21	0.40	0.74	5.90	161.28

Considering the above discussions, we designed two inlets with the same width for the co-flow of the water sample and the clean buffer into our devices, respectively from their inner inlet and the outer inlet (Figure 2-1 A-B). Close to the main curved microchannel, we added indicators at 10^o angle intervals to make the investigation of flow possible at known lengths of the channel. At the outlet of the curved microchannel, we added a small straight microchannel with a length of 0.5cm to eliminate the effect of Dean vortices before collecting the samples from the outlets (Figure 2-1C). Two outlets were designed for the device. The inner outlet was designed with a smaller width in order to collect the switched clean buffer at the highest possible fluid purity and target large particle concentration. The outer outlet was designed wider to make for the total width of the

curved channel. The two outlets were separated with a small gap to effectively separate the fluid near the inner wall from the one adjacent to the outer wall (Figure 2-1C). According to the large particle focusing and fluid switching criteria defined above, the optimized channel geometry was determined to be a semicircular channel with a radius of R=1.185 cm with a width and height of 300 and 70 µm, respectively.

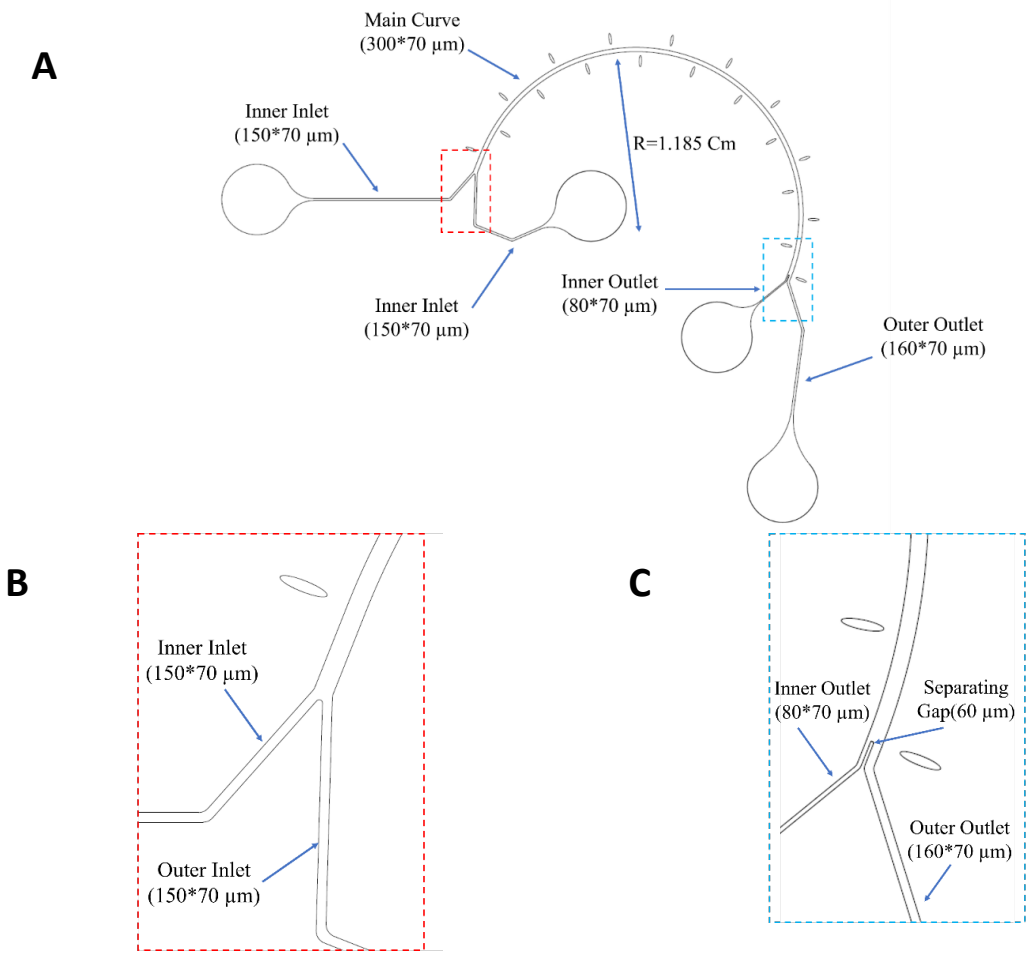

Figure 2-1 Example of a curved microchannel centrifuge device designed in this thesis. (A) It consisted of two inlets, a curved microchannel, a short straight microchannel, and two outlets. The inner inlet and outer inlet were used for the injection of water sample and a clean buffer, respectively. The water sample contained microparticles and or bacteria. (B) Channel inlets with identical width. (C) Channel outlets with different widths in the inner and outer outlet and the designed gap between them for enhancing the separation of fluid streams.

One crucial consideration in the design of microfluidic channel networks pertains to hydraulic resistance ($R_{hyd}=\Delta p/Q$, where Δp is pressure difference across the channel and Q is the volumetric

flow rate) [107]. Hydraulic resistance has significance in this thesis as branching and networking happens in our design at the channel's inlet and outlet as well as in parallelization of the curve channels. An elevated hydraulic resistance within the channel results in opposition to the flow, consequently altering the flow rates and division of fluids at channel junctions. For instance, if the hydraulic resistances in the branches of a channel are not uniform like the outlet of our device, the flow within channels featuring lower hydraulic resistance will assume dominance.

Hydraulic resistance depends significantly on the channel dimensions, with higher channel lengths and smaller channel cross sections contributing to elevated R_{hyd}. For instance, the hydraulic resistance of a rectangular channel can be calculated using equation (2-1) where μ is the fluid viscosity and w, h and L are the channel width, height, and length, respectively [108]. Since the widths of the two outlets in our device were intentionally made different to achieve higher solution exchange efficiency and better purity for particle separation, we tried to design the lengths of the outlet microchannels in a way that flow in both outlets experience the same R_{hyd}. To have similar hydraulic resistances at the two outlets, we had to increase the length of the outer outlet which is wider in comparison with the inner outlet (Figure 2-1C). We disregard pressure losses at the outlet points since both outlets have identical conditions. Additionally, we mitigate pressure losses by avoiding sharp bends in the outlet channels and do not account for the impact of pressure losses at these bends.

$$R_h \approx \frac{12\mu L}{wh^3(1-\frac{0.63h}{w})} \tag{2-1}$$

Another factor that needs to be taken into consideration is the comparison between diffusion and convection flows in the curved channel. Ideally, diffusion should be avoided to maintain the water sample and the clean buffer separated from each other at the outlets. In inertial microfluidic

devices, Reynolds number is low which leads to low levels of turbulence, therefore mixing will occur only by diffusion [109]. Peclet number is a dimensionless number that represents the ratio of convection rate to diffusion rate (equation 2-2) [110]. In equation (2-2), U represents the axial velocity of fluid, L is the length scale of the flow and D is the diffusion constant.

$$Pe = \frac{Convective\ Rate}{Diffusion\ Rate} = \frac{UL}{D} \tag{2-2}$$

When $Pe \geq 1$, diffusion is negligible, and we can neglect the effect of diffusion mixing. In our designed device in Figure 2-1C, Pe number is in the order of 10^5. Based on the designed channel dimensions and the velocity of the fluid in the channel we can claim that there is a negligible diffusion of sample into the clean buffer and the injected sample from the inner inlet will switch to the outer wall at the outlet as an effect of secondary flow and during this process, there will not be a considerable diffusive mixing of the sample and the clean buffer.

As discussed in Chapter 1, one of the most effective methods to increase the flow rate of microfluidic devices is in-plane and out-of-plane parallelization of devices such as the one shown in Figure 2-2. In this method, several microfluidic devices are connected together in parallel and the flow rate of the parallelized device would be the sum of the flow rates of each device. In order to decrease the number of fluid access ports on the device, identical channel inlets and outlets of the parallelized device should be interconnected and interfaced with the operating pumps. One of the parameters that makes it challenging to parallelize curved microfluidic devices is linking similar fluidic access ports as they are surrounded by channels. In objective 1 of the thesis, we used two different methods of arraying (rectangular in Figure 2-2 a-c and polar in Figure 2-2 d-f) and in each method, we completed our investigation by doubling the number of microfluidic devices at each step. We started our study by two-curve devices, then doubled it to four-curve

devices, and finally, based on our device geometry and the maximum number of devices that could be fit on one silicon wafer, we expanded the design to eight curved devices.

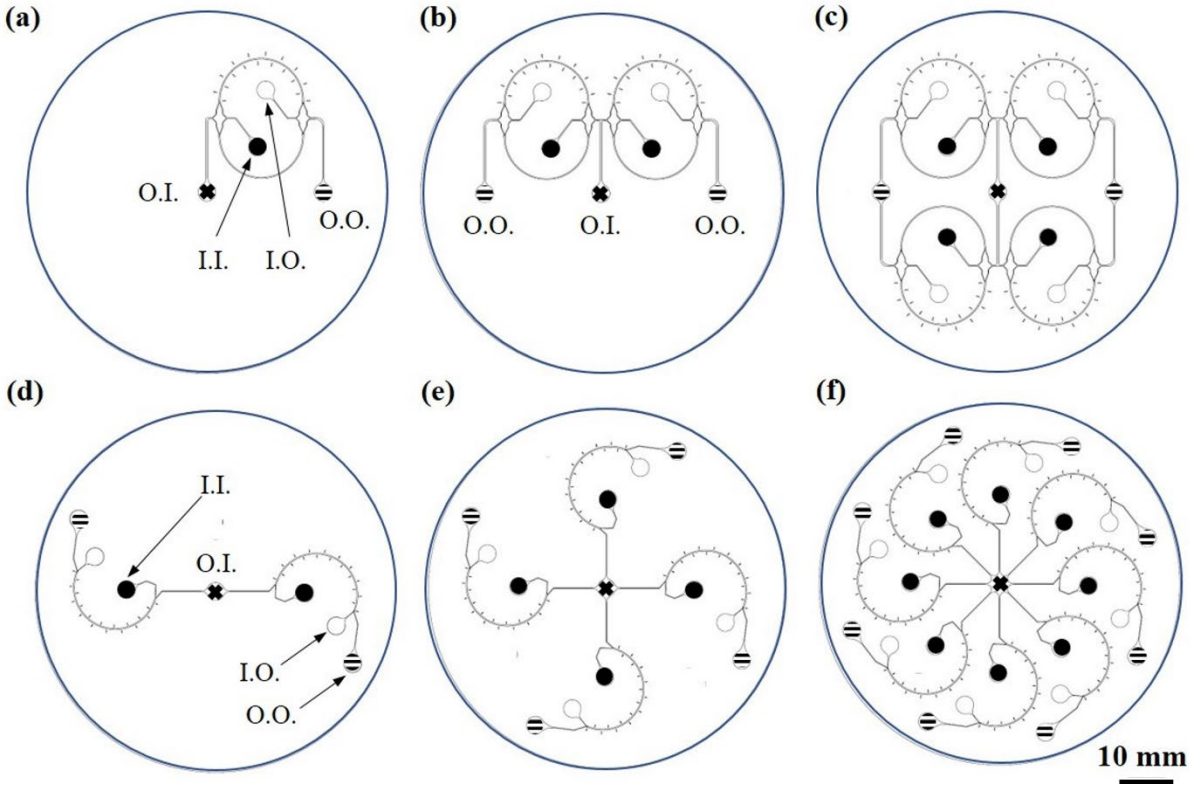

Figure 2-2 Two different methods for centrifuge microfluidic device parallelization. Fluidic ports with similar functions are connected to each other. (a-c) Rectangular parallelization of devices. In each step number of curves are doubled. (d-f) Radial array of curved microfluidic channels. Number of curves starts at 2 and reaches 8 in two steps.

2.3 Device Fabrication

Microfluidic centrifuge devices were made by replica molding of polydimethylsiloxane (PDMS) over photoresist-patterned silicon master molds as schematically shown in Figure 2-3. This methodology was previously developed and optimized in Dr. Pouya Rezai's lab. To prepare the master mold, we used standard photolithography [111]. First a 4 inch diameter silicon wafer purchased from Wafer World Inc., FL, USA was cleaned with acetone, methanol, and DI-water, followed by drying using air gun flow hotplate treatment for 2min at 120°C. The clean and dried

substrate was plasma oxidized in a plasma machine (Harrick Plasma, PDC-001, NY, USA) to make the surface of the silicon wafer hydrophilic. Then, the prepared substrate was centered on a spin coater machine. SU8-2075 negative photoresist was purchased from Microchem Corp., MA, USA, and poured on the silicon wafer. Each variant of SU8 has its specific properties like viscosity and sensitivity to UV light which affect the fabrication process like speed and time of spinning and exposing. The speed and time of spinning depends on the desired thickness of the photoresist layer which for our device design, with the channels' height of 70 μm, was determined to be 3000 rpm for 30 seconds based on the supplier recipe [112]. After spinning, the accumulated SU8 was removed from the edges of the silicon wafer using glass slides. For soft baking, we put the SU8-coated silicon wafer on hotplates at 70º and 95ºC for 5 and 9 minutes, respectively. The SU8 coated and prebaked silicon wafer was then aligned with a photomask containing the design of the device and exposed using an ultraviolet exposing machine (UV-KUB 2, KLEO, France). The UV-exposed substrate was post-baked at 70º and 90ºC for 2 and 7 minutes, respectively. After post-baking, the unexposed parts of the SU8 were removed using an SU8-developer solution. At this step, the master mold was ready for hard baking at 200ºC for 20 minutes.

To fabricate the microfluidic devices using the master molds, we used soft lithography [113]. PDMS (Sylgard 184 kit, Dow Corning, MI, USA) base solution was mixed with its curing agent at a ratio of 10:1. The mixture was degassed in a desiccator and poured on the master mold. After baking at 70 ºC for 2 hours, the cured PDMS was peeled off from the silicon wafer. The fluidic access ports were punched with a biopsy punch (Harris Uni-Core punch). To form enclosed channels, the PDMS layer was bonded on a glass substrate using the oxygen plasma machine. The bonded device was then heated at 70 ºC for 20 minutes to enhance bonding. For connecting the device to the syringes, we used Tygon tubes (L/S 14 and 16, Masterflex, USA).

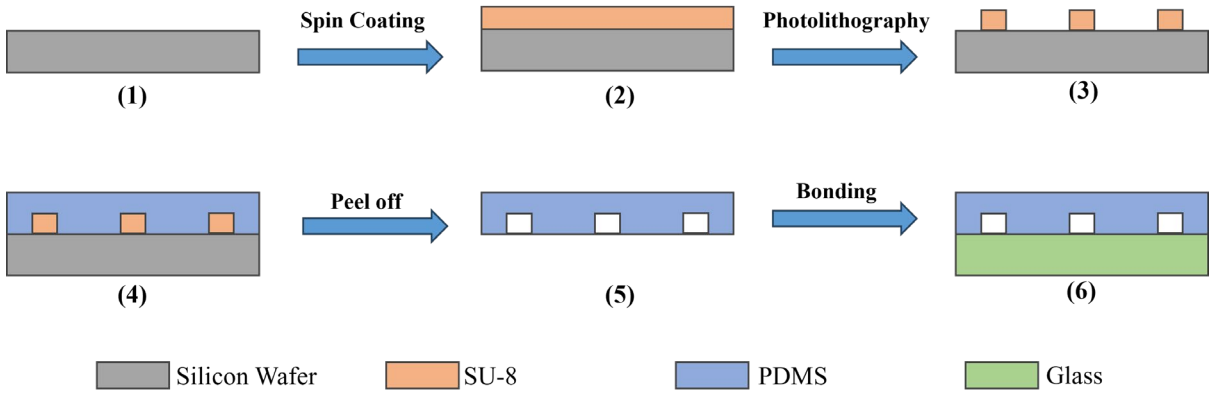

Figure 2-3 Microfluidic device fabrication process. (1-3) Photolithography steps for preparation of silicon wafer replication master mold. (4-5) Soft lithography procedure for PDMS device fabrication against the master mold. (6) Bonding the fabricated PDMS layer on a glass substrate for making enclosed microchannels.

2.4 Experimental Procedures

Solution exchange and separation of particles were studied under an inverted microscope (Bioimager, BIM 500FL, Canada) with a camera (Point Grey, FLIR, Canada). Different microfluidic centrifuge devices with various numbers of curved channels and layers were used in the setup (Figure 2-4 A-C). For performing an experiment, we connected the two inlets of our device in Figure 2-4D (top) with tubing and connections to two identical 60 mL syringes. To infuse the fluids through the device, we used a dual syringe pump (KD Scientific - Legato® Syringe Pumps). One of the syringes contained DI water as the clean buffer, connected to the outer inlets of the device. The other syringe contained 15% v/v trypan blue in water solution to be visualized under the microscope. This syringe was connected to the inner inlet of the device. Particle and *Salmonella* bacteria suspensions were also infused into the device from this inlet. Co-flows of the water streams inside the device were video recorded at 5x magnification.

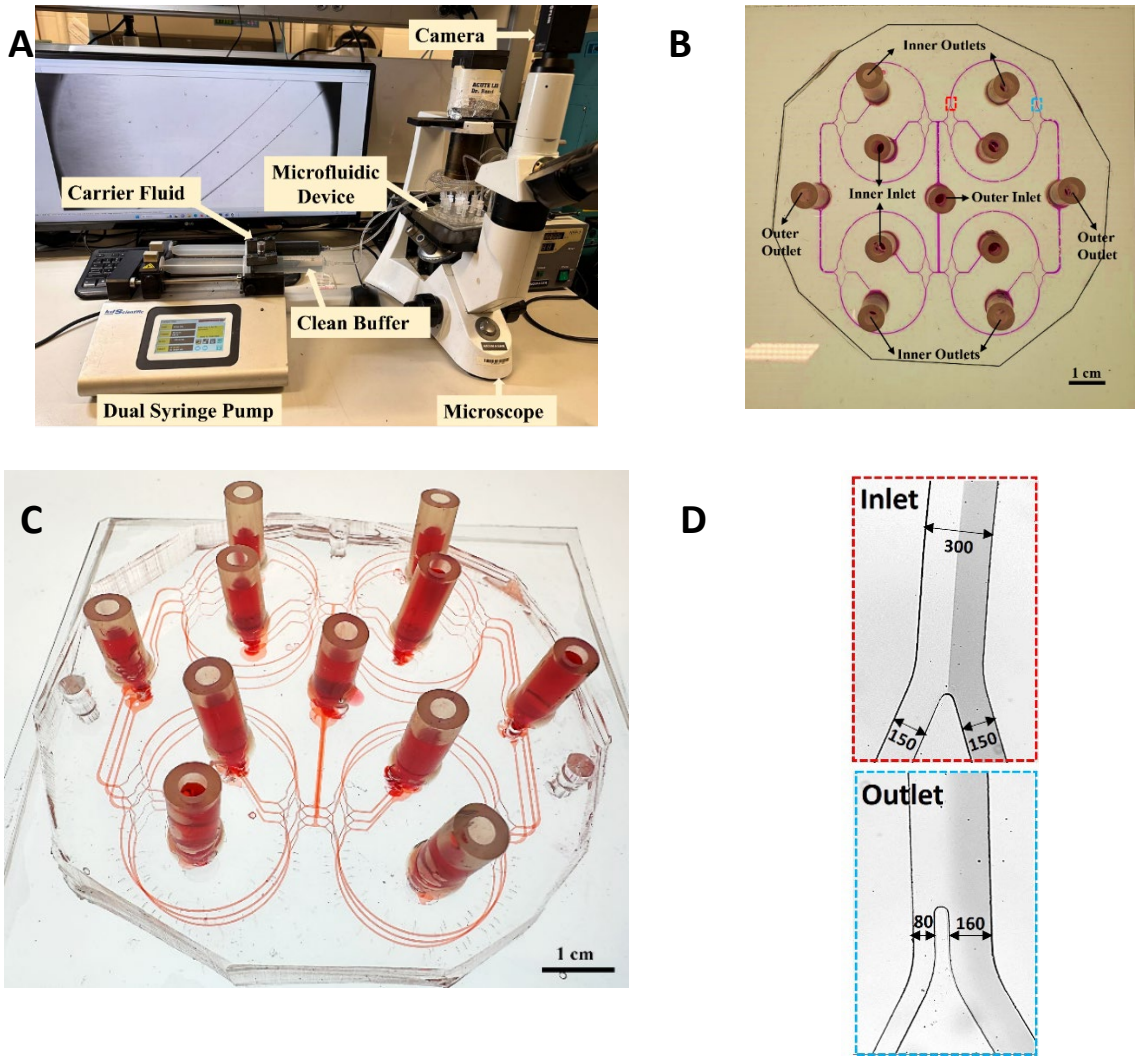

Figure 2-4 Experimental setup and various microfluidic devices. A) Experimental setup consisting of a dual syringe pump, a microscope, and the microfluidic device. B) Photograph of a 1-layer 8-curve channel device with inlets and outlets. C) Photograph of a 3-layer 8-curve channel device. D) Microscope image of the device inlets (top) and outlets (bottom) under an inverted microscope with co-flows of pure and trypan blue dyed waters.

The flow rates used at the two inlets were adjusted to be identical and ranged from 0.6 to 1 mL/min per inlet. For particle and bacteria studies, the particles or bacteria were added to the carrier solution at a specific concentration and infused through the inner inlet. The samples from the outlets were collected for analysis. The solution exchange efficiency for devices with 2 curves is described in section 2.6 while for devices with more than 2 curves, solution exchange was

examined by spectrophotometry measurement of trypan blue in the outlet samples, described below.

2.5 Off-Chip Analysis of Solution Exchange and Particle Separation

The purity of buffers collected from the outlets of the device can be calculated by measuring the concentration of trypan blue in the solution, which was done by spectrophotometry [89]. Here, we used a single monochromator UV-2600 spectrophotometer (Shimadzu Corporation, Japan) to measure the absorbance of different trypan blue concentrations in DI water (i.e., 0% v/v to 2% v/v) and establish a calibration curve. Absorbance is calculated from the ratio of intensity of transmitted light through the sample to the intensity of transmitted light through blank. This ratio results in a dimensionless number and is reported in arbitrary units (a.u). The peak absorbances data were used to find a correlation for the concentration of trypan blue in the solution. As shown in Figure 2-5a, for a range of 0.25-2.0% v/v, the peak absorbance in the visible range occurred at an approximate wavelength of ~ 590 nm. As illustrated in Figure 2-5a, the peak absorbance increases for the higher trypan blue concentrations in DI water. These absorbance peaks were then used to fit a linear correlation with respect to the trypan blue concentration in DI water.

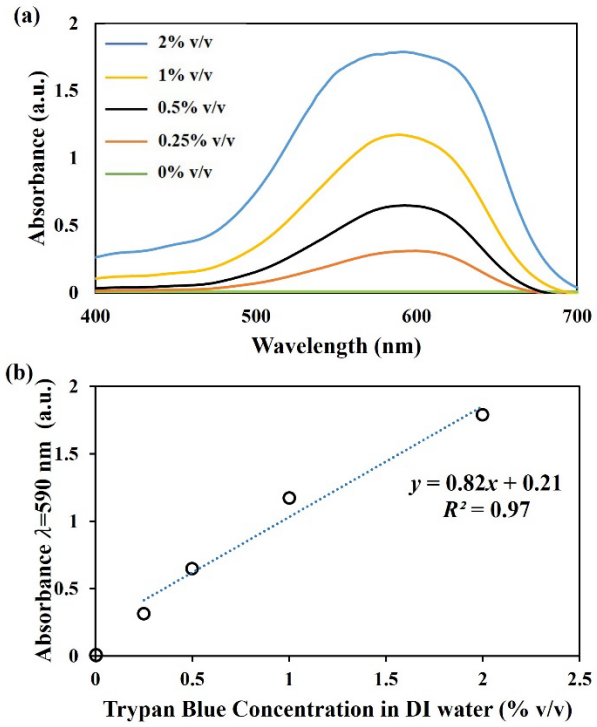

Figure 2-5 UV-VIS spectrometry of trypan blue spiked water. (a) Absorbance of different trypan blue concentrations in DI water in the visible range. Here, 0% v/v concentration indicate the undyed DI water. (b) Peak absorbance at 590nm vs. trypan blue concentration in DI water. A linear correlation could be fitted over the 0.25-2.0% v/v range with R^2 = 0.97.

As shown in Figure 2-5b, the calibration line in equation 2-3 could be used to predict the trypan blue concentration in the collected samples from the outlets with R^2 = 0.97.

$$y = 0.82\,x + 0.21 \qquad (2\text{-}3)$$

Here, y stands for the peak absorbance of the solutions and x indicates the trypan blue concentration of the collected samples at the channel outlets.

The linear correlation in equation 2-3 is used to calculate the trypan blue concentrations and the solution exchange efficiency at the channel outlets. For this, the purity of clean buffer, showing the solution exchange efficiency in equation (2-4), was defined as the percentage concentration of trypan blue in the sample collected from the inner outlet in respect to the concentration of trypan blue in the inner inlet (15% v/v trypan blue in DI water).

$$Solution\ Exchange\ Efficiency = (1 - \frac{Trypan\ Blue\ Concentratio\ in\ Inner\ Outlets\ Sample}{Trypan\ Blue\ Concentration\ in\ Inner\ Inlet}) \times 100 \quad (2\text{-}4)$$

Microparticle separation in the microfluidic device was analyzed by counting the number of particles in each outlet using a hemocytometer (Marienfeld Superior, Germany) under an inverted microscope (Leica, Wetzlar, Germany). The experiments were replicated three times, with particle counts conducted three times for each sample to determine mean values and standard deviations. Particle sorting efficiency was defined as the ratio of particles in the target outlet to the total collected particle count from outlets as shown in equation (2-5).

$$Efficiency = \frac{Number\ of\ Target\ Particles\ in\ the\ Selected\ Outlet}{Total\ Number\ of\ Target\ Particles\ in\ All\ Outlets} \times 100 \quad (2\text{-}5)$$

Another studied parameter was the purity of particle separation. It was calculated using the number of target particles (i.e., 10 μm) in each outlet divided by the total number of collected particles (5 μm, and 10 μm) in the respective outlet as illustrated in equation 2-6.

$$Purity = \frac{Number\ of\ Target\ Particles\ in\ the\ Selected\ Outlet}{Total\ Number\ of\ All\ Particles\ in\ All\ Outlets} \times 100 \quad (2\text{-}6)$$

To investigate bacteria separation from particles, we counted colony forming units within serially diluted samples obtained from the device outlets, following standard plate culturing and colony counting procedures [114]. The efficacy of bacteria separation was quantified as the percentage of *Salmonella* bacteria present in each outlet.

Solution exchange efficiencies, particles' collection efficiencies, and purities are reported as the average, and standard deviations of three measurements for three different tests (i.e., total of 9 measurements).

2.6 On-Chip Analysis of Solution Exchange

To analyze the solution exchange performance of the devices on-chip (using microscope images acquired from running experiments), we captured videos from co-flows of trypan-blue solution and DI-water in 2-curve devices and analyzed the videos using the ImageJ software (National Institutes of Health, Bethesda, Maryland, USA) [115]. Images along the channel at 10 degree intervals were acquired from the videos, with examples of the inlet, middle section, and the outlet of the device shown in Figure 2-6A. Gray color intensities, c_i, were measured along assessment lines crossing the curved microchannel at 10-degree intervals as shown in Figure 2-6B [89].

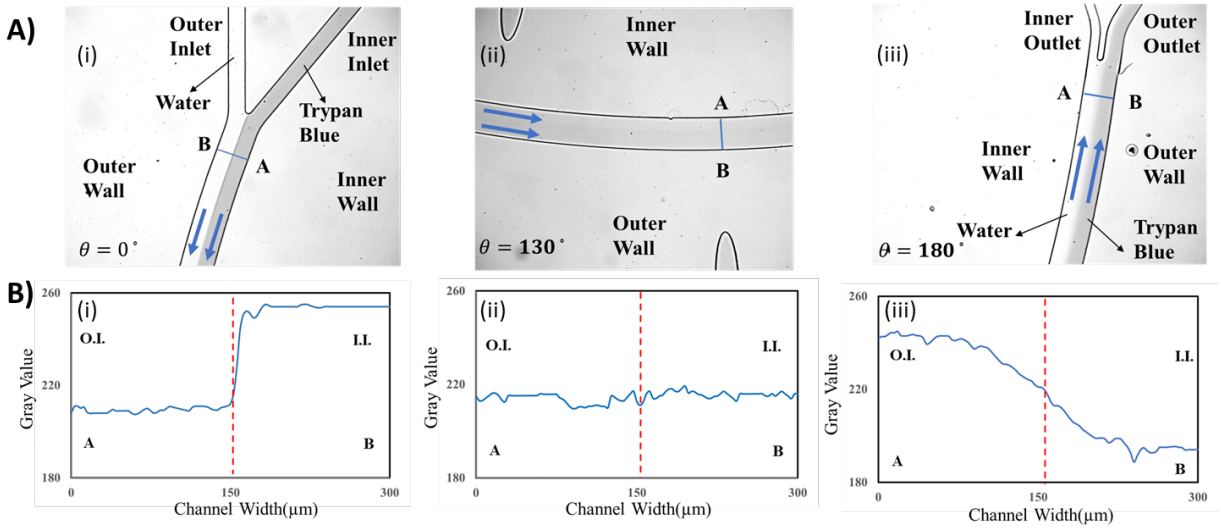

Figure 2-6 Co-flow images of trypan blue water and undyed DI water at a total flow rate of Q = 3.2 mL/min along the microchannel length at three angular locations (i.e., $\theta = 0°, \theta = 130°, and\ \theta = 180°$). A) Microscopic images taken from the curve inlet (i), the middle of the channel (ii) and the curve outlet (iii). B) The gray value intensities, c_i, along the line A-B at the cross sections of A along the channel.

The standard deviation of the color intensities at each assessment line A-B was calculated using equation (2-7).

$$\sigma = \sqrt{(1/N)\sum_{i=1}^{N}(c_i - \bar{c})^2} \tag{2-7}$$

Where N is the number of pixels along the assessment line, c_i is the intensity at each pixel and, $\bar{c}$ is the average intensity along the assessment line.

We defined the switching index (SI) as the normalized standard deviation of the intensity along each assessment line with respect to the maximum standard deviation within the curved part of the channel (equation (2-8)) [89].

$$SI = {}^{\sigma}/_{\sigma_{max}} \tag{2-8}$$

In equation (2-8), σ_{max} is the maximum amount of standard deviation among all the assessment lines in the channels which is expected to occur at the inlet of the channel where the dyed and un-dyed solutions were completely separated (Figure 2-6A).

At the channel inlet (Figure 2-6Ai and Bi), dyed and undyed water create a distinct interface, leading to the maximum standard deviation of color intensities (σ_{max}) which also corresponds to $SI = 1$. At the middle section of the microchannel (Figure 2-6Aii and Bii), the secondary flow components caused by Dean vortices tend to enhance mixing in the transverse direction (perpendicular to the main flow direction), causing a uniform distribution of color intensities along the width of the microchannel which corresponds to σ_{min}, and SI_{min}. Finally, at the channel outlet (Figure 2-6 Aiii and Biii), the first solution exchange is completed which corresponds to a local maximum value for σ and SI.

CHAPTER 3

In-Plane Parallelization of Microfluidic Centrifuge Devices

3 In-plane Parallelization of Microfluidic Centrifuge Devices

3.1 Solution Exchange Inside In-Plane Parallelized Dual-Curve Devices

We started our curve-channel arraying experiments by testing the device shown in Figure 2-2a which consisted of two curved channels made in PDMS, arrayed rectangularly in parallel and plasma bonded to a glass substrate. As a reminder, the device dimensions were w=300 μm, h=70 μm, R=1.185 cm. Co-flows of pure and trypan blue dyed DI water were run through the curved microchannels at different flow rates using a dual syringe as shown in Figure 2-4A. An inverted microscope equipped with a camera was used to record the co-flows at 5x magnification. Co-flows in the 2-curve device were supplied at total flow rates of Q_t = 2.4, 3.2, and 4.0 mL/min (subscriptions t means total flow rate of the device including the inner and outer inlets of all curved channels in one device). These flow rates correspond to $Q_{o.i.}$= $Q_{i.i.}$ = 0.6, 0.8, and 1.0 mL/min for

each stream of flow in each curve, respectively (subscriptions o.i and i.i mean outer inlet and inner inlet, respectively). In this scenario, there is a limited diffusion-based mixing due to the substantial axial velocity (V_{ax} ~ 0.95-1.59 m/s) within the curved channel. Video recordings of the experiment were transferred to the ImageJ software [115] for fluid behavior analysis as discussed in the methods chapter.

Figure 3-1 depicts distinct channel cross-sections delineating the inlet, midsection, and outlet of the device in an example experiment. The color intensity values, correlated with the channel width, are illustrated for both the upper segments (a-c) and the lower segments (d-f) of the rectangular design featuring two curves. These observations are made under conditions where liquids are concurrently flowing, maintaining a flow rate of $Q_{i.o}$=$Q_{o.i}$ = 0.8 mL/min within each inlet (equivalent to total flow rate of Q_t = 3.2 mL/min).

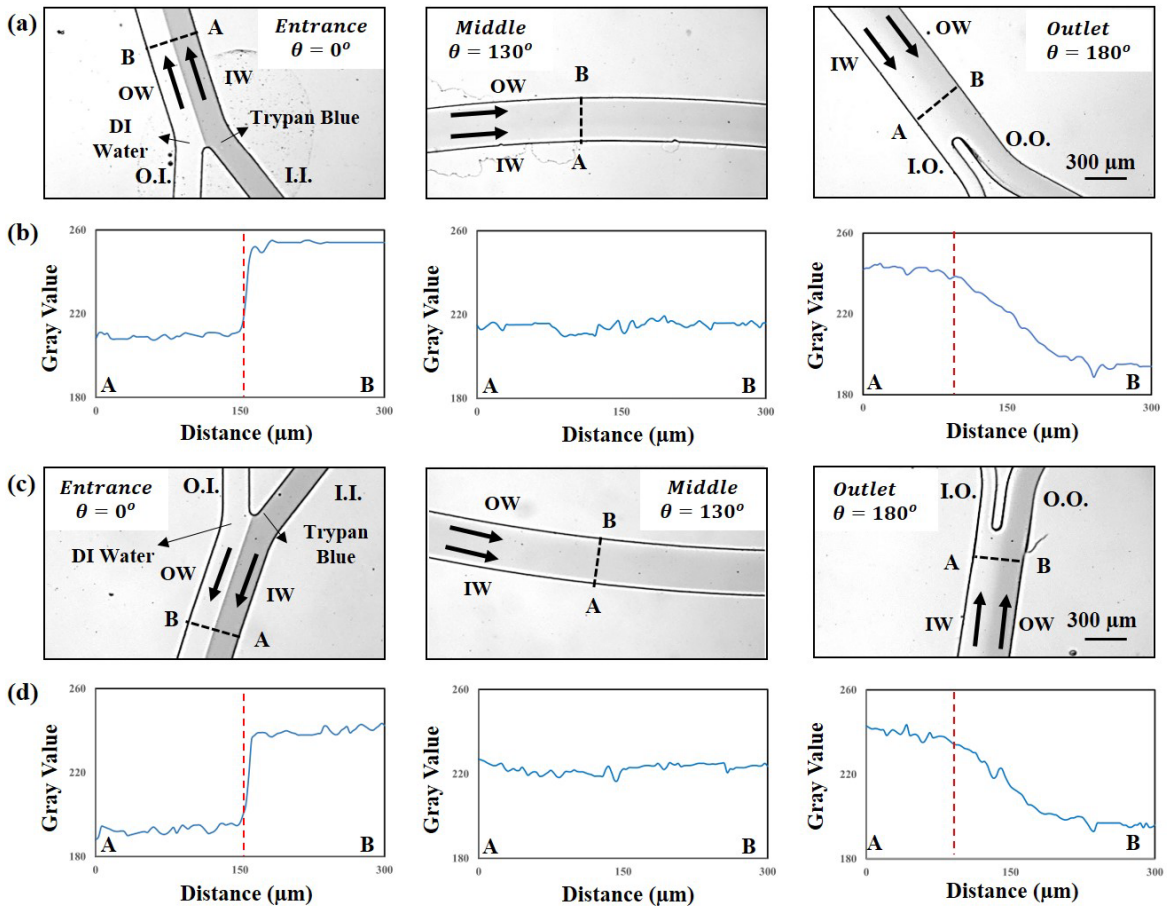

Figure 3-1 Co-flow images of trypan blue and undyed DI water at a total flow rate of Q_{curve} = 1.6 mL/min along each of the two curved microchannels (R = 1.18 cm, w×h=300×70 µm^2) in the (a) top and (c) bottom curves of the 2-curve device (rectangular array). (b) and (d) represent the color intensity values along the line A-B in the top and bottom curve of the device, respectively. II: inner inlet; OI: outer inlet; IO: inner outlet; OO: outer outlet; IW: Inner Wall; OW: Outer Wall

As shown in Figure 3-1a (and Figure 3-1c) at the channel inlet, two distinct co-flows of dyed and undyed DI water create the maximum standard deviation (σmax), which corresponds to the SI = 1. At the channel middle section, two co-flow layers sandwiched each other due to the secondary Dean flow in the curvature and created a more uniform color intensity distribution alongside the channel width (σmin resulting in SImin). Finally, fluid recirculation at the channel outlet interchanged the location of co-flows, indicating a 0.5 fluid recirculation or one fluid switch with a local maximum value for the switching index. The required length to reach to the first fluid recirculation is denoted is Ls. As illustrated in Figure 3-1, the fluid recirculation pattern is similar

in both curves in the rectangular arrayed curved device, which indicates the uniform performance of this centrifuge.

3.2 Quantification of Fluidic Switching Index (SI) in Dual-Curve Channel Devices with Rectangular and Polar Arrays

Initially, we investigated if parallelization of the curved channel from one [8], [89] to two curves, in rectangular and polar arrays, would impact the quality of fluid recirculation and switching in our device. The effect of flow rate on the fluid recirculation at the channel outlet was studied. Figure 3-2 illustrates the effect of flow rate on the switching index alongside the channel length in one of the curves when the co-flows are supplied through the 2-curved devices with rectangular (Figure 3-2a), and polar (Figure 3-2b) configurations.

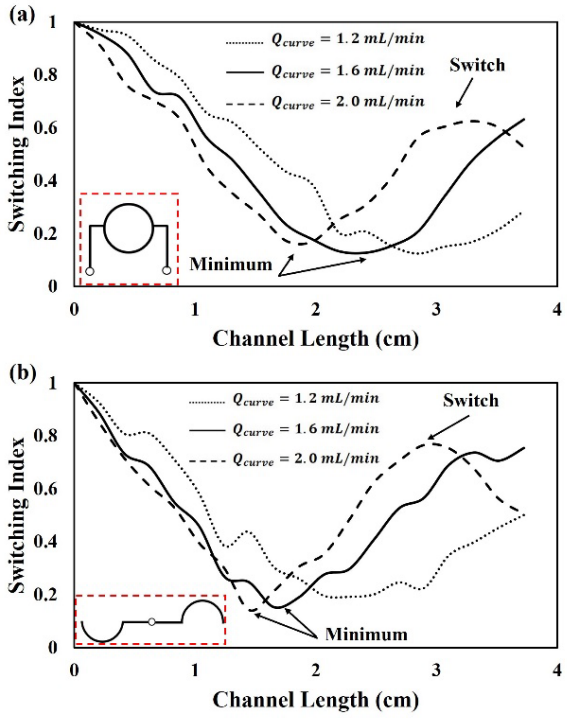

Figure 3-2 The switching index (SI) of dyed and undyed DI water flowing through the top curve of (a) rectangular and (b) polar devices with 2 curves at three different flow rates. The first local maximum of SI indicates the fluid switching point due to the Dean flow recirculation.

As shown in Figure 3-2a, when the co-flows are supplied with a total flow rate of Q_t = 4.0 mL/min (where subscription *t* means the total flow rate through the channel includicg all inlets and outlets of total device and i.e., Q_{curve} = 2 mL/min in each curve, where subscription curve means the flow rate of one curved microchannel including the inner and outer inlet), the first fluid switch occurred before the curved channel outlets at Ls = 3.28 cm. The flow rate of Q_{curve} = 2 mL/min theoretically provides one full switch by the channel outlet in a single-curve channel device. We hypothesize that due to the addition of another channel in parallel in this experiment, variations in the hydraulic resistance of the device may have led to pressure distribution differences with a single-curve channel device, hence causing minor changes to the fluid switching performance of the arrayed device. The variations in pressure distribution could stem from alterations in the cross-sectional dimension of the channels caused by the flexibility of PDMS under high pressure. Another potential factor might be the interaction of fluid streams in devices that are parallelized. When the total flow rate was decreased to Q_t = 3.2 mL/min (i.e., Q_{curve} = 1.6 mL/min in each curve), the switching index reached the local maximum at the channel outlet (L_s = 3.72 cm, Ls indicated the length of the channel that a complete switch happens) and a complete switch was achieved. A complete switch occurs when the carrier fluid moves towards the outer wall while the clean buffer stream flows alongside the inner wall. At this point, the fluid flows are once again separated, and we observe a peak in the standard deviation of color intensities on the graph representing the Switching Index (SI). Upon further decrease in the flow rate to Qt = 2.4 mL/min (Q_{curve} = 1.2 mL/min in each curve), the fluid recirculation was delayed and the complete fluid switch did not happen by the channel outlet at $L_{channel}$ = 3.72 cm ($L_{channel}$ shows the total length of each curved microchannel).

As shown in Figure 3-2b for the 2-curved device with polar configuration, at a total flow rate of Qt = 4.0 mL/min, the complete fluid switch occurred before the channel outlet at Ls = 2.9 cm. When the flow rate decreased to Qt = 3.2 mL/min (Q_{curve} = 1.6 mL/min in each curve) the switching index reached to the local maximum of SI = 0.75 at the channel outlet, which indicated the 0.5 fluid recirculation. A further decrease in the total flow rate down to Qt = 2.4 mL/min (Q_{curve} = 1.2 mL/min in each curve), resulted in incomplete fluid switch at the channel outlet as indicated in Figure 3-2b. Therefore, we concluded that despite the theoretical optimum flow rate of Qt = 4.0 mL/min, in both rectangular and polar configurations (Figure 3-2a and 3-2b), the complete fluid switch occurs at the total flow rate of Qt = 3.2 mL/min (Q_{curve} = 1.6 ml/min in each curve). This total flow rate was chosen for the continuation of this study in the next sections.

The interaction of fluid streams in parallelized devices might be another reason for this deviation from the theoretical flow rate. Another parameter that might be considered as a reason of reduction in the flow rate is deformation of flexible PDMS channel`s wall by the applied pressure from the fluid. Moreover, as the applied correlations for V_{De} and SI calculations are empirical, the effects of some parameters such as the channel material, wall roughness and environmental effects are not considered accurately.

3.3 Effect of Rectangular vs Polar Parallelization Architecture on Solution Exchange Efficiency

Solution exchange efficiencies at the device outlets were investigated when the dyed and undyed solutions were co-flown at $Q_{i.i}$ = 0.8 mL/min (where $Q_{i.i}$ is the flow rate at the inner inlet) in each inlet in 2-curve, 4-curve, and 8-curve devices with rectangular and polar configurations. Here, the collected samples from the inner outlets were examined with the UV-VIS spectrophotometer, and

the equivalent trypan blue concentrations in each sample were calculated using the calibration curve presented in Equation 2-3 and Figure 2-5. As illustrated in Figure 3-3, for the co-flows in the 2-curve device with rectangular and polar array the solution exchange efficiencies were 96.6% ± 0.3%, and 92.7% ± 0.3%, respectively. Moreover, for the co-flows in the 4-curve device, the device with the rectangular array resulted in a purity of 96.7% ± 0.4%. However, the solution exchange efficiency in the 4-curve device with a polar array dropped to 84.7% ± 0.40%. Finally, in the 8-curve device with the rectangular array, the collected sample at the inner outlets indicated a solution exchange efficiency of 96.8% ± 0.5%. On the other hand, the efficiency in the 8-curve device with a polar array was 89.8% ± 0.7%.

Our study revealed that the efficiency of solution exchange remains relatively consistent in the rectangular array setup. However, in devices employing a polar array, we observed fluctuations in this efficiency. When comparing the results between devices using rectangular and polar arrays, we noticed a lower solution exchange efficiency in devices utilizing the polar parallelization method. Specifically, we found that the solution exchange efficiency decreased by 4%, 12%, and 7% in polar-array devices with 2, 4, and 8 curves, respectively. The poor performance of the polar devices might be because of the increased number of inlet and outlet ports compared to the rectangular array. This increase in the number of outlets could potentially increase the unfavorable flow fluctuations inside the curves and eventually lead to lower solution exchange efficiencies. The diminished efficacy of solution exchange in polar arrayed devices can also be attributed to the gradient in channel height extending from the device's center towards its edges. This gradient arises due to centrifugal forces exerted during the fabrication of the master mold. Specifically, the thickness of the SU8 coating is notably greater along the edges of the silicon wafer as compared to its central region.

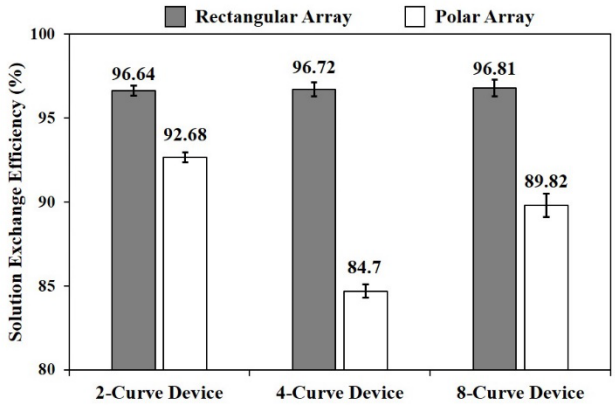

Figure 3-3 Solution exchange efficiency at the channel inner outlet for 2-curve, 4-curve, and 8-curve microdevices with rectangular and polar arrays, when the solutions are co-flown at Q_{curve} = 1.6 mL/min in each curve (Q_t = 3.2, 6.4, and 12.8 mL/min, respectively).

Overall, based on the presented results in Figure 3-3, and due to a better performance consistency in the rectangular device, we decided to pursue particle separation investigations in the curved devices with a rectangular array.

3.4 Particle Separation Efficiency and Purity in Rectangular Arrayed Centrifuge Devices

Particle separation efficiencies were initially examined in the 2 curve microdevice with a rectangular array. Figure 3-4a shows the separation efficiencies when the singleplex particle solution (5 µm or 10 µm) is co-flown from the inner inlet alongside a clean buffer at a flow rate of $Q_{i.i}$ = 0.8 mL/min per each inlet (i.e., Q_t = 3.2 mL/min). Here, the larger 10 µm particles mostly remained close to the channel inner wall under the dominant effect of the inertial lift forces and were collected with an average efficiency of 98.93% ± 0.91% in the inner outlet. On the other hand, the smaller 5 µm particles were under the dominant effect of the Dean drag and were transferred towards the channel outer wall. As illustrated in Figure 3-4a, only 21.74% ± 3.72% of

the 5 µm particles remained close to the channel inner wall. Meanwhile, 78.25% ± 3.72% of the smaller particles were collected from the outer outlets.

Later on, duplex sample (mixture of 5µm, and 10µm particles) purities were examined inside the rectangular array microdevices with 2, 4, and 8 curves at total flow rates of $Q_{i,i}$ = 1.6, 3.2, and 6.4 mL/min of carrier fluid (i.e., total flow rate within the device are Q_t = 3.2, 6.4 and 12.8 mL/min, respectively). Figure 3-4b shows the sample purities for 10 µm and 5 µm particles collected from the inner and outer outlets, respectively. Here, the larger 10 µm particles were collected from the inner outlet with a purity of 85.02% ± 1.28% in the 2-curve device. The sample purity for the 10 µm particles increased in the 4-curve and 8-curve devices to 91.30% ± 3.75% and 92.83% ± 1.47%, respectively. This indicates that lower number of smaller 5 µm particles remained close to the channel inner wall in the 4, and 8 curve devices. Although, the solution exchange efficiencies were comparable in all devices with the rectangular array (Figure 3-3), smaller particles might have traveled more uniformly towards the outer wall which resulted in the increased sample purity in Figure 3-4b.

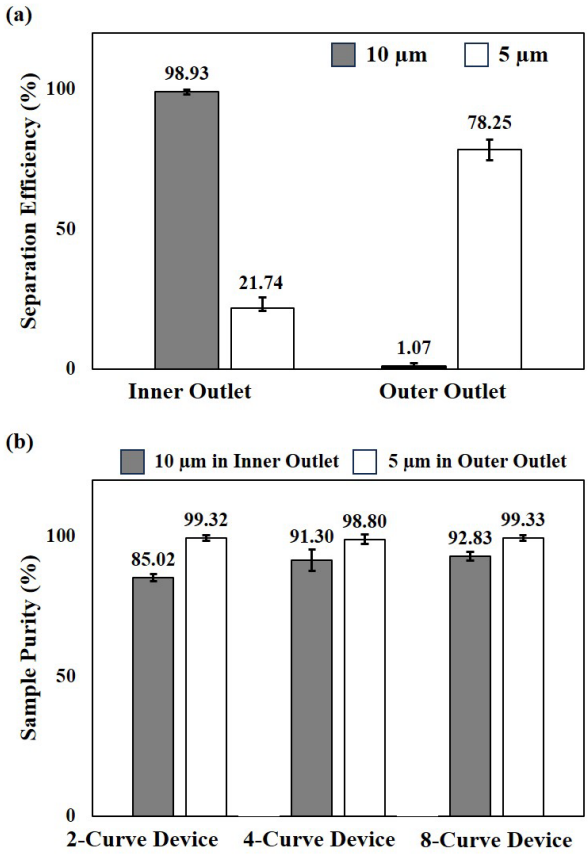

Figure 3-4 Separation efficiency and sample purity of the in-plane rectangular parallelized devices (a) single-plex separation efficiencies for 5 µm, and 10 µm particles at the channel outlet, when the particle solutions were co-flown alongside a clean buffer at Qcurve = 1.6 mL/min in the 2-curve device (Qt = 3.2 mL/min) with rectangular array. (b) Sample purities for 5 µm, and 10 µm particles for duplex sample in the inner and outer outlets, respectively, when co-flown simultaneously at Q_{curve} = 1.6 mL/min in the 2-curve, 4-curve, and 8-curve microdevices with rectangular array. Error bars indicate the standard deviations of measurements for three different samples.

We also investigated the sample purities for 5 µm particles at the outer outlets. As shown in the Figure 3-4b, 5 µm particles were collected with an efficiency of 99.32% ± 0.97%, in the outer outlets of the 2-curve device. Sample purities for the 5 µm particles in the 4-curve and 8-curve devices were similarly close with 98.80% ± 1.70% and 99.33% ± 0.94%, respectively. Here, since the larger 10 µm particles were under the dominant effect of inertial lift forces, they were mostly collected at the inner outlets. Therefore, the Dean drag only managed to push the smaller 5 µm particles towards the outer wall. This resulted in high sample purities for smaller particles at the outer outlets.

Comparing the findings of our current investigation with those from our previous study in single curve devices [116], it is obvious that our new 8-curve parallelized device demonstrates a notable improvement. The parallelized device exhibits an enhanced capacity to retain 5 μm particles within the carrier fluid, achieving a purity level of 99.32% ± 0.97%. This shows an improvement over previous metrics which had a purity of 98% ± 0.7%. Furthermore, our innovative device showed better performance for washing 10 μm particles and inertially focusing them at the inner outlet. This parallelization enhanced the sample purity at the inner outlet from 86 ± 2% in the prior device to 92.83 ± 1.47% in our current configuration. Last but not least, these enhancements are achieved along with a 640% increase in the processing flow rate.

3.5 Conclusion

In summary, in this chapter we investigated the effect of flow rate and channel geometry on the performance of a particle washing process in a curvilinear microchannel system. Solution exchange and particle separation efficiencies were investigated with various flow rates in 2, 4, and 8 curve microchannels with rectangular and polar arrays. We found the optimum working condition and channel configuration and demonstrated a high throughput, high efficiency particle separation and washing process. We achieved solution exchange efficiencies of > 96.6 % for high flow rates up to 12.8 mL/min. An efficient particle separation was demonstrated at a total flow rate of 12.8 mL/min for 5 μm and 10 μm particles, where larger 10 μm particles were separated close to the channel inner wall with efficiencies > 98%. Sample purities of 92.83% and 99.33% were also achieved for 5 μm and 10 μm particles in the outer and inner outlets, respectively.

CHAPTER 4

Out of Plane Parallelization of Microfluidic Centrifuge Devices

4 Out Of Plane Parallelization of Microfluidic Centrifuge Devices

4.1 Effect of substrate material on solution exchange

Typically, and as demonstrated in the previous chapter for planar centrifuge devices, microfluidic devices are constructed through plasma bonding of a PDMS layer containing microchannels onto a glass substrate, as illustrated in the initial version of our device [8]. However, the out-of-plane parallelization necessitates the bonding of three layers of PDMS microchannels atop one another. In this configuration, if the entire device were bonded to glass, the substrate material would be glass for the first layer, while the second and third layers would entirely consist of PDMS. Accordingly, we first explored the impact of substrate material on solution exchange. To conduct this investigation, two 2-curve devices with rectangular arrays were fabricated. The first device was directly plasma bonded onto a glass substrate, while the second one was bonded onto a glass substrate coated with a thin layer of PDMS. Dyed and undyed water samples were co-flown at a total flow rate of Q_t = 3.2 mL/min (i.e., $Q_{i.i} = Q_{o.i}$ = 0.8 mL/min per curve inlet and $Q_{i.i}$ $Q_{o.i}$ refers

to the flow rate at the inner and outer inlet respectively) and the solution exchange was monitored through both devices qualitatively and quantitatively (Figure 4-1). As shown in Fig. 4-1 A and B, when the substrate was glass, the solution exchange (switch) occurred at the outlet cross section, evidenced by *SI* having a local maximum at 180 degrees along the curvature of the microchannel. This was in good agreement with our findings in Chapter 3. However, when the substrate was PDMS (Figure 4-1 C and D), the solution exchange occurred prior to reaching the outlet cross section. This is evidenced by *SI* exhibiting a local maximum at an angle less than 180 degrees.

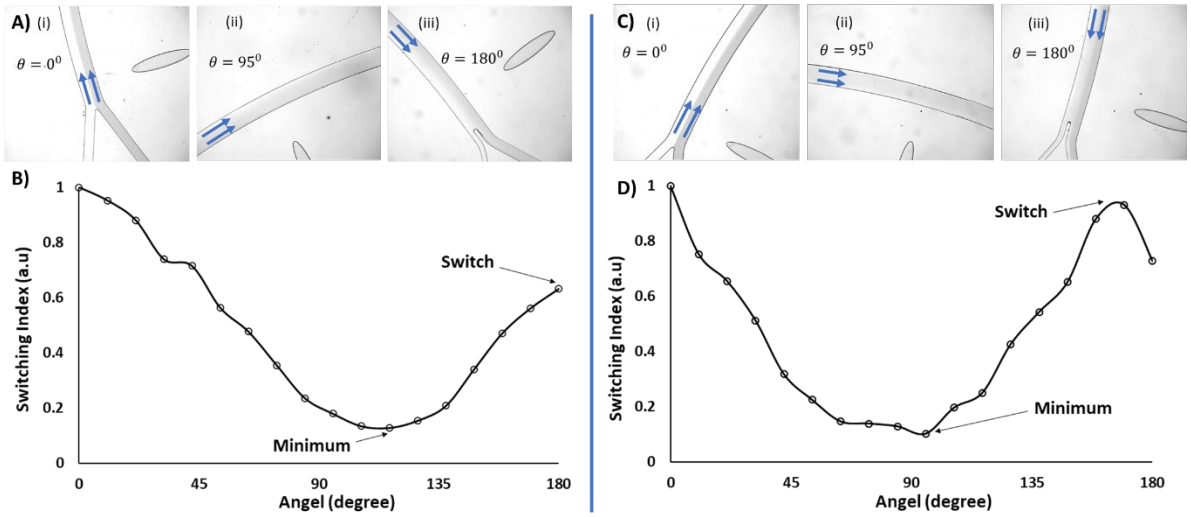

Figure 4-1 Effect of substrate material on solution exchange at a constant flow rate of Q=0.8 mL/min per inlet. A 2-curve device was bonded on glass (A-B) and PDMS-coated glass substrates (C-D). Microscopic images were taken to demonstrate the interface between the trypan blue and undyed DI water at different positions along the channel curve at the inlet (i), middle of the channel (ii), and the outlet (iii) on devices bonded on glass (A), and PDMS (C), respectively. Monitoring the alteration of SI along the channel curve demonstrated that when the substrate was glass (B), the solution exchange (switch) occurred at the outlet cross section, leading to a local maximum at 180 degrees for SI. However, when the substrate was PDMS (D), the solution exchange occurred prior to reaching the outlet cross section, causing SI to reach a local maximum at an angle less than 180 degrees.

We concluded that the change in substrate material from glass to PDMS may have altered the interactions between the flowing fluids and the channel walls. PDMS is known for its flexibility and hydrophobic nature, which can influence fluid-wall interactions compared to the more rigid and hydrophilic glass. These variations in surface characteristics can impact the development of

Dean vortices and subsequently affect the position of the solution exchange as demonstrated in Fig. 4-1. Similarly, the effect of channel wall rigidity on particle focusing has been recently demonstrated in zigzag channels involving Dean flow [117]. This discrepancy was linked to changes in the hydraulic diameter caused by the expansion of PDMS microchannels at high flow rates. Notably, we demonstrated that altering just one side of the channel (the substrate) significantly impacts solution exchange in curved microchannels. To ensure uniform solution exchange across all layers of the multilayer device in this chapter, we consistently employed PDMS-coated glass as the substrate for the parallelized devices in all experiments. However, this required determination of the flow rate that would provide a complete switch exactly at the outlet of such all-PDMS devices.

4.2 Effect of Flow Rate on Solution Exchange of All-PDMS Centrifuge Devices

In accordance with the discourse presented in Chapter 3, our investigation revealed the optimal flow rate for devices affixed to glass substrates to be 0.8 mL/min per each inlet. However, it was recognized in section 4.1 that altering the foundational substrate from glass to PDMS will inevitably induce a shift in the optimized flow rate required for achieving high-efficiency solution exchange. Consequently, our ensuing examination will delve into elucidating the impact of flow rate variations on solution exchange efficiency within PDMS-based devices.

The maximum solution exchange efficiency is achieved when the fluid switching concludes at the device outlet, corresponding to the local maximum of the switching index (SI_{max}). However, the Dean flow-based half fluid recirculation point called the switching point depends on the flow rate. Therefore, the effect of flow rate on solution exchange in a 2-curve device was investigated by

measuring the switching index (SI) along the channel length at different inlet flow rates ranging from 0.6 to 0.9 mL/ min (Figure 4-2A).

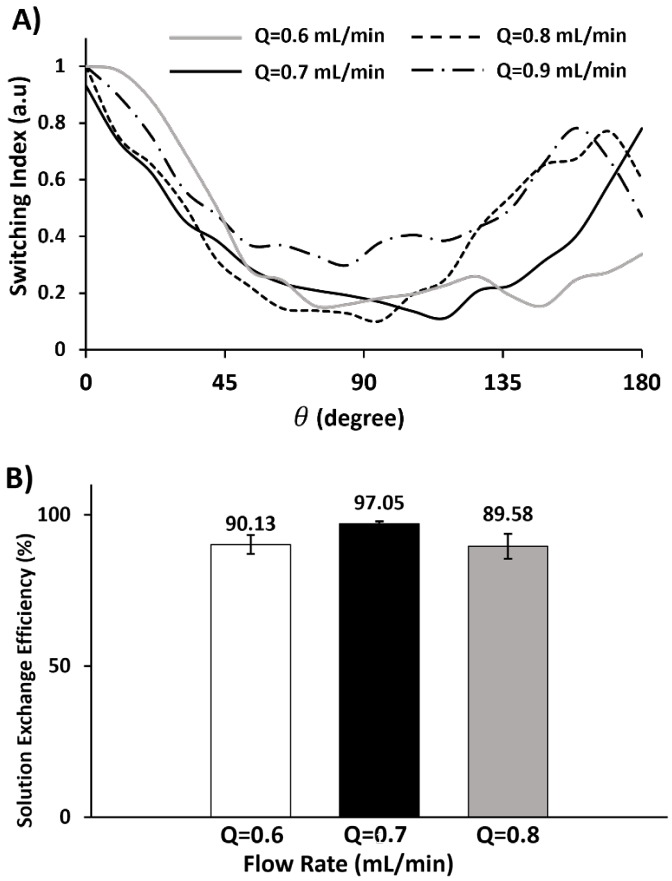

Figure 4-2 Effect of flow rate on solution exchange in a PDMS-based 2-curve channel device bonded on a PDMS coated glass substrate. A) Switching index at different angular distances along the curvature of the device at different flow rates. B) Solution exchange efficiency at different flow rates.

At an inlet flow rate of $Q_{i.i}$ = 0.9 mL/min (i.e., a total flow rate of $Q_t = 2\times1.8=3.6$ mL/min in the 2-curve device), the first fluid switch occurred before the curved channel outlet at $\theta = 160°$ (Figure 4-2A). Upon reducing the inlet flow rate to $Q_{i.i}$ = 0.8 mL/min (i.e., a total flow rate of Q_t = 3.2 mL/min in the 2-curve device), the solution exchange was delayed such that the switching index reached the local maximum at $\theta = 170°$, yet it was prior to the channel outlet. Decreasing the inlet flow rate to $Q_{i.i}$ = 0.7 mL/min (i.e., a total flow rate of Q_t = 2.8 mL/min in the 2-curve device) led

to additional delay in the solution exchange, with the local maximum of the switching index positioned at the channel outlet at θ = 180°. A further reduction in the inlet flow rate to $Q_{i.i}$ = 0.6 mL/min (i.e., a total flow rate of Q_t = 2.4 mL/min in the 2-curve device) resulted in the absence of a fluid switch at the channel outlet.

The efficiency of solution exchange was also assessed at three different flow rates (Figure 4-2B). As expected, a maximum solution exchange efficiency of 97.05 ±0.79% was attained at an inlet flow rate of $Q_{i.i}$ = 0.7 mL/min, where the switching point coincided with the channel outlet at θ = 180°. The solution exchange efficiency decreased to 90.13 ± 3.11% and 89.58 ± 4.15% at inlet flow rates of $Q_{i.i}$ = 0.6 mL/min and $Q_{i.i}$ = 0.8 mL/min, respectively. Accordingly, for a device with PDMS walls all around, an optimum flow rate of $Q_{i.i}$ = 0.7 mL/min was selected for continuation of the experiments.

4.3 Effect of In-Plane Parallelization on Solution Exchange Efficiency in All-PDMS Centrifuge Devices

In Chapter 3, we delved into the examination of the impact of parallelization on the efficiency of solution exchange for devices featuring 2 to 8 curves, each possessing a single layer bonded onto a glass substrate in polar or rectangular arrays. In this instance, our focus shifted to scrutinizing the influence of in-plane parallelization on devices exhibiting 2 to 8 curves, while concurrently altering the foundational substrate to one coated with PDMS on glass.

While parallelization enhances the operational flow rate, it is imperative to scrutinize its impact on device performance, encompassing the efficiency of solution exchange and particle separation. In-plane parallelization was achieved by increasing the number of curved channels within a single-layer device arranged in a rectangular array. Dyed and undyed solutions were co-flown at an

optimal flow rate of $Q_{i.i}$ = 0.7 mL/min per inlet in 2-curve, 4-curve, and 8-curve devices, resulting in a switching point coinciding with the channel outlet at θ = 180°. The samples obtained from the inner outlets underwent UV-VIS spectrophotometry, and the corresponding concentrations of trypan blue in each sample were determined utilizing the calibration curve outlined in equation 2-3. Solution exchange efficiencies of 97.05 ± 0.79%, 95.84 ±2.38%, and 96.02 ±0.66% were achieved for 2-curve, 4-curve, and 8-curve devices, respectively (Figure 4-3). The increase in the number of curves from 2 to 8 significantly elevated the total operational flow rate from Q_t = 2.8 ($Q_{i.i}$ =$Q_{o.i}$ = 0.7 mL/min per inlet) to 11.2 mL/min in an 8-curve device, without a noteworthy alteration in solution exchange efficiency.

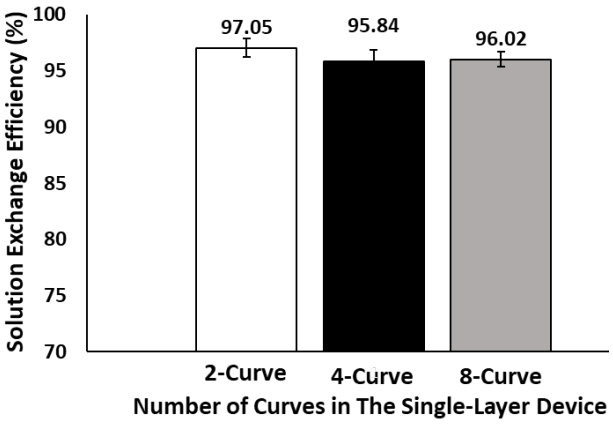

Figure 4-3 Effect of in-plane parallelization on solution exchange efficiency for 2- to 8-curve PDMS devices bonded on PDMS-coated glass substrates.

4.4 Effect of In-Plane Parallelization on Solution Particle Separation in All-PDMS Centrifuge Devices

Particle behavior was initially examined using single-plex samples containing 5 µm or 10 µm microparticles each at a concentration of 10^5 particles/mL in a 2-curved device. Particle suspensions were co-flown from the inner inlet alongside a clean buffer from the outer inlet at an

inlet flow rate of $Q_{i,i}$ = 0.7 mL/min (i.e., a total flow rate of Q_t = 2.8 mL/min in the 2-curve device). As demonstrated in Figure 4-4A, the larger 10 μm particles mostly remained close to the channel inner wall under the dominant effect of the inertial lift forces and were collected with an average efficiency of 98.99% ± 1.43% in the inner outlet. On the other hand, the smaller 5 μm particles were under the dominant effect of the Dean drag and were transferred towards the channel outer wall, with an average efficiency of 93.45% ± 1.82% in the outer outlet. This behavior could be predicted by comparing R_f, the ratio of lift force (F_L) to the Dean drag force (F_D), for 5 μm and 10 μm microparticles within the 2-curved device at Q_t = 2.8 mL/min (i.e., Q_{curve} = 1.4 mL/min). As per Equation 1-7, R_f for 5 μm and 10 μm microparticles was calculated to be 0.62 and 4.97 respectively, providing a rationale for the observed particle behavior.

Increasing the number of curves to 8 in a single layer device significantly enhanced the throughput of the device while maintaining its performance. The separation efficiencies were measured to be 98.97 ± 1.45% and 91.64 ± 2.1% for 5 μm and 10 μm microparticles, respectively (Figure 4-4B).

Separation purity was then examined for a duplex particle solution, comprising a mixture of 5 μm and 10 μm particles at the same concentration (10^5 particles/mL), in both 2-curve and 8-curve single-layer devices. As illustrated in Figure 4-4C, microparticles in the duplex solution exhibited comparable behavior to the singleplex solution. Larger microparticles predominantly moved towards the channel's inner wall, while smaller microparticles were directed toward the channel's outer wall, influenced primarily by the inertial lift forces acting on larger particles and the Dean drag forces acting on smaller microparticles. A 2-curve device provided separation purities of 96.2 ± 3.63% and 98.24 ± 2.48% for 10 μm and 5 μm microparticles in a duplex sample, respectively. Notably, the separation purity remained unchanged when the number of curves increased to 8 in the parallelized device, despite the operational flow rate being significantly increased.

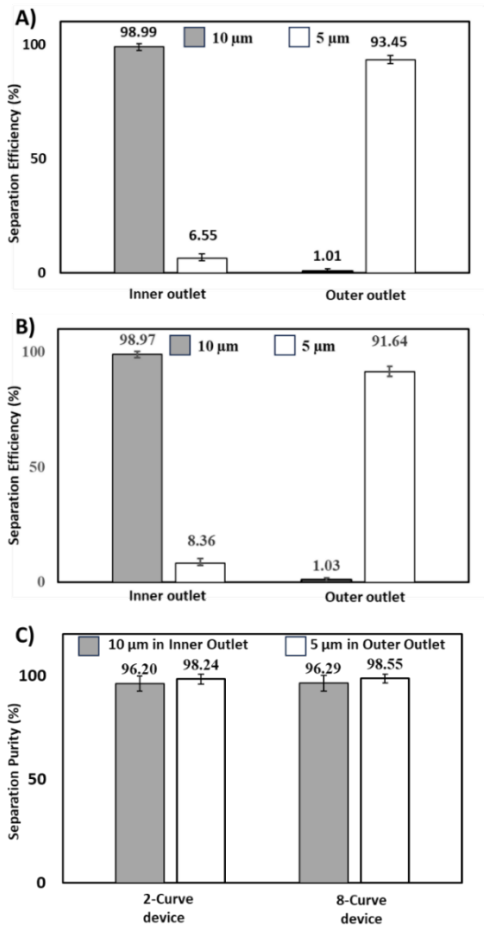

Figure 4-4 Effect of in-plane parallelization on particle separation within all-PDMS rectangularly arrayed centrifuge devices. A) Particle separation efficiency for a 2-curve device bonded on a PDMS substrate using single-plex samples containing 5 µm and 10 µm microparticles. B) Particle separation efficiency for an 8-curve device bonded on a PDMS substrate using single-plex samples containing 5 µm and 10 µm microparticles. C) Separation purity of 5 µm and 10 µm microparticles collected from the outer and the inner outlets, respectively, in 2-curve and 8-curve devices using duplex samples.

4.5 Effect of Out-of-Plane Parallelization of Microfluidic Centrifuge Devices on Solution Exchange Efficiency

To further increase the throughput of the device, out-of-plane parallelization was accomplished by plasma bonding three 8-curved devices on top of each other (Figure 4-5A). This configuration resulted in an increase in the total operational flow rate to Q_t = 33.6 mL/min (i.e., Q_{curve} =1.4 mL/min per curve and $Q_{i,i}$=$Q_{o,i}$ =0.7 mL/min per inlet).

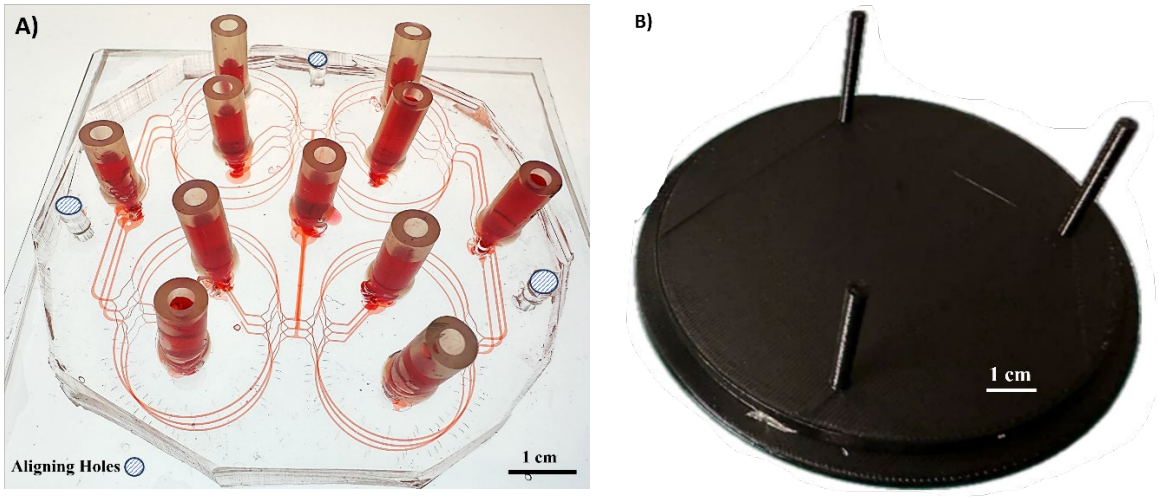

Figure 4-5 Our-of-plane rectangularly arrayed 24-curve microfluidic centrifuge device. A) Photograph of a 3-layer microfluidic centrifuge device with 8 interconnected curved microchannels in each layer. Blue circles show the punched holes designed for aligning the layers. B) 3D-printed fixture used for aligning the three PDMS layers before bonding.

To attain a uniform hydraulic resistance across all inlets and outlets of the device, ensuring the proper alignment of the fluidic access holes is imperative. To achieve this, three aligning marks were fabricated on the silicon master molds. Subsequent to the PDMS layers' detachment from these replication molds, the alignment marks were carefully punched with a biopsy punch, as depicted in Figure 4-5A. A dedicated 3D-printed fixture as illustrated in Figure 4-5B was meticulously designed to facilitate the alignment of layers. This fixture incorporates three pins that traverse through the previously punched aligning holes. Using this fixture, the fabrication process involved plasma bonding of the three layers of PDMS devices onto a glass substrate coated with PDMS. This procedure resulted in the creation of a multi-layered device, as depicted in Figure 4-5A.

The effect of out-of-plane parallelization on solution exchange efficiency was investigated both with and without the presence of microparticles in the samples (Figure 4-6). Out-of-plane parallelization resulted in a solution exchange efficiency of 96.69% ± 0.28% and 96.32% ± 0.29%

with and without the presence of microparticles, respectively. This indicates that the presence of microparticles does not have a discernible impact on the solution exchange efficiency in the device. Additionally, the solution exchange efficiency in the multilayer device was nearly equivalent to that of an 8-curve single-layer device, demonstrating that out-of-plane parallelization did not negatively impact the solution exchange efficiency.

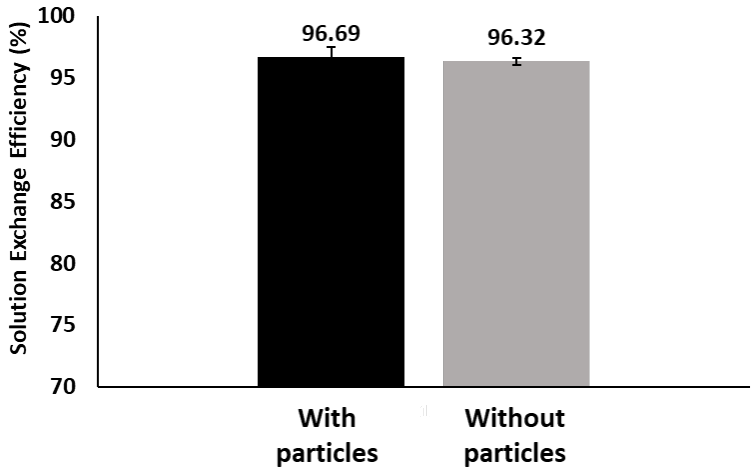

Figure 4-6 Solution exchange efficiency in a multilayer 24-curve microfluidic centrifuge device bonded on a PDMS-covered glass substrate with and without the presence of microparticles in the solutions.

4.6 Effect of Out-of-Plane Parallelization of Microfluidic Centrifuge Devices on Particle Separation

Separation efficiency of microparticles was assessed in the three-layer high-throughput device of Figure 4-5A using single-plex samples containing microparticles (Figure 4-7A). Microparticle suspension and the clean buffer were introduced into the device from the inner and the outer inlets, respectively. The total inlet flow rate for each sample was 16.8 mL/min ($Q_t = 16.8 \times 2 = 33.6$ mL/min) leading to an optimal inlet flow rate of 0.7 mL/min per inlet of each curve. Similar to what was observed for a single layer device, 10 µm microparticles remained close to the inner wall

of the curve and were collected from the inner outlets with a total separation efficiency of 99.67 ± 0.46%. This separation efficiency was slightly higher than what was observed for a single layer 8-curve device. Moreover, the operational flow rate was three times higher in the out-of-plane parallelized device. On the other hand, 5 μm microparticles were primarily influenced by the Dean drag forces which transferred them toward the channel outer wall. Separation efficiency for smaller 5 μm microparticles collected from the outer outlets was calculated to be 90.29 ± 3.11%.

Duplex sample purities were assessed within the multilayer device at a total inlet flow rate of 16.8 mL/min for microparticle suspensions and the clean buffer (Q_t = 16.8×2 = 33.6 mL/min). This examination was conducted both with and without trypan blue in the sample to determine whether the dye could potentially influence the results. Figure 4-7B illustrates the sample purities for 10 μm and 5 μm particles collected from the inner and outer outlets, respectively. In the absence of dye in the sample, larger 10 μm particles were obtained from the inner outlet with a purity of 90.72% ± 2.13%, while smaller 5 μm particles were collected from the outer outlet with a purity of 97.41% ± 1.91%. Introducing the dye into the samples slightly elevated the sample purities to 93.37% ± 1.74% and 98.55% ± 2.05% for 10 μm and 5 μm particles, respectively; however, the changes were insignificant. When compared to a single-layer 8-curve device (Fig. 4-4C), the separation purity for 10 μm particles only decreased by approximately 5% in the multilayer device (Fig. 4-7B), while the sample purity for 5 μm particles remained consistent in both devices.

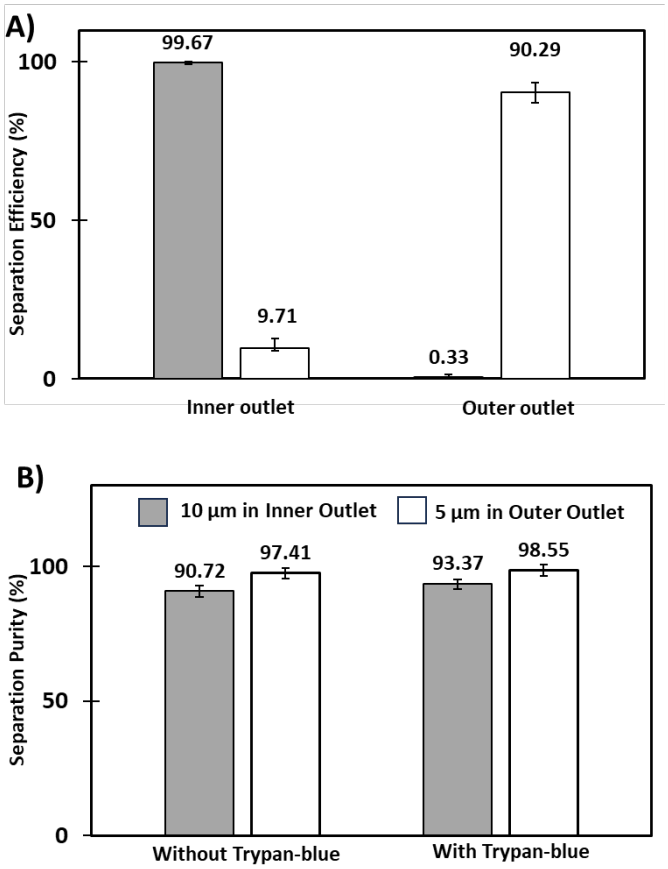

Figure 4-7 Effect of out-of-plane parallelization on particle separation. (A) Separation efficiency of the multilayer high-throughput device using single-plex samples containing 5µm and 10 µm microparticles. (B) Separation purity of the multilayer high-throughput device for 10 µm and 5 µm particles collected from the inner and outer outlets with and without the presence of trypan blue.

4.7 Application of the 24-Curve Microfluidic Centrifuge Device: High-Throughput Solution Exchange and Separation of Microparticles from *Salmonella* Bacteria

Conventional filtration and centrifugation methods are prone to bacterial cell damage and irreversible agglomeration of cells due to compaction [118], [119]. Moreover, they are not suitable for automated and continues sample processing due to membrane clogging and fouling issues in filtration and labor-and energy-intensiveness of centrifugation [118], [119]. On the other hand, the widespread acceptance of microfluidic technology in industries has been hindered primarily by the lower throughput of conventional microfluidic systems, despite the numerous unique advantages

they bring to the table as discussed in Chapter 1. Previous attempts for increasing the throughput of the microfluidic filtration or sorting devices, sometimes, came at the expense of decreasing the efficiency of the process and purity of the samples [99], [120]. Parallelization has predominantly been showcased in spiral microchannels featuring microchannels with single inlet and multiple outlets [99], [100]. It is important to highlight that having fewer inlets simplifies the setup and improves user-friendliness in parallel spiral channels with one inlet per curve [100]. However, this comes with a trade-off, as these devices, while proficient in microparticle filtration and fractionation, lack the capability for solution exchange due to the absence of an inlet for clean buffer. This limits their applications when continuous particle washing and transferring them to a clean buffer is needed. For instance, transferring DNA carrying microparticles from PCR-inhibitors and simultaneously washing them into clean water for detection using a portable PCR thermocycler was demonstrated using a single curve microchannel [5]. Here, we explored whether the in-plane and out-of-plane parallelization presented in this study can significantly enhance the throughput of particle-bacteria assays without compromising efficiency.

After a comprehensive parametric analysis of our microfluidic centrifuge devices characteristics, considering both in-plane and out-of-plane parallelization, we investigated its efficacy in simultaneously separating surrogate particles from *Salmonella* bacteria and exchanging carrier and clean buffer solutions. Initially, behavior of the *Salmonella* bacteria and the solution exchange was investigated without microparticles. A solution of *Salmonella* in LB broth with a concentration in the order of 10^5 CFU/mL was passed through the inner inlets at a total inlet flow rate of 16.8 mL/min. Simultaneously, PBS, as the target clean buffer, entered the outer inlets at the same flow rate, resulting a total flow rate of $Q_t = 16.8 \times 2 = 33.6$ mL/min passing through the multilayer device. This is equivalent to $Q_{curve} = 1.4$ mL/min passing through each curve (0.7 mL/min per curve inlet).

The flow rates were kept similar to the case of DI water and trypan blue since the viscosity and density values were comparable with DI water. A similar experiment was performed by introducing 10 μm microparticles, with a concentration of 10^5 Particles/mL, into the *Salmonella* bacterial solution, creating a duplex mixture.

Quantifying the *Salmonella* bacteria concentration in collected samples from the outlets revealed that 99.17 ±0.42% of *Salmonella* bacteria were collected from the outer outlet when no microparticles were present in the sample (Figure 4-8A). The introduction of microparticles into the sample did not alter the bacteria's behavior in the device as most of the bacteria were still collected from the outer outlet. This occurred because *Salmonella*, with an effective diameter smaller than 5 μm [121], possessed a very small R_f value. Therefore, it was primarily under the influence of the Dean drag forces, transporting it towards the outer outlet. Conversely, 10 μm microparticles were inertially focused at the inner wall of the curved microchannel due to their higher R_f value as discussed before.

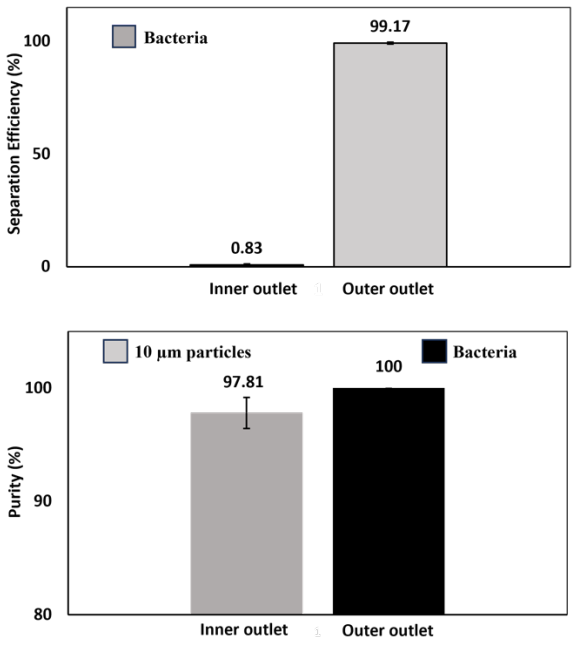

Figure 4-8 High-throughput solution exchange and separation of microparticles from bacteria at a total inlet flow rate of 16.8 mL/min for the clean buffer and bacteria suspension (i.e., a total flow rate of Q_t = 16.8×2=33.6 mL/min passing through the multilayer device). A) Bacteria separation efficiency demonstrated that 99.17% of bacteria were collected from the outer outlet using a singleplex solution. B) Separation purity of the multilayer high-throughput device for duplex solution containing 10 µm particles and bacteria which were collected from the inner and the outer outlets, respectively.

Comparing concentrations of bacteria and microparticles at the outlets of the device for a duplex sample demonstrated a high purity of 100% and 97.81 ± 1.37% for bacteria and 10 µm microparticles in the outer and inner outlets, respectively (Figure 4-8B). Hence, in-plane and out-of-plane parallelization significantly increased the throughput of the device while maintaining a high separation efficiency and purity. Importantly, culturing bacteria post-collection from the outlet revealed that the device had no impact on bacteria survivorship. Moreover, the addition of more layers to the device has the potential to further increase the throughput.

4.8 Conclusion

We presented a multilayer microfluidic device for high-throughput solution exchange and microparticle separation, catering to applications which need processing large sample volumes at high flow rates. This was achieved through in-plane and out-of-plane parallelization of 24 curved microchannels, as microfluidic centrifuge units, within a compact three-layer configuration. Each microfluidic centrifuge unit integrated Dean flow recirculation of two fluids with selective inertial focusing of target particles. This integration facilitated the isolation of target particles from non-target particles and their subsequent washing into a clean buffer with high throughput and efficiency. The effect of substrate material (i.e., glass or PDMS) and flow rate on the performance of particle washing process in single and multilayer devices containing different numbers of curved microchannels (i.e., 2-curve, 8-curve, and 24-curve devices) were investigated. We demonstrated high throughput and efficiency in separating and washing particles for both singleplex and duplex samples containing one or two distinct sizes of microparticles, respectively. We attained solution exchange efficiencies exceeding 96% at total inlet flow rates of up to 5.6 mL/min and 16.8 mL/min for single-layer and multilayer devices, respectively.

Efficient particle separation was exhibited at a total inlet flow rate of 16.8 mL/min for both 5 μm and 10 μm particles. The larger 10 μm particles remained near the channel inner wall and were collected from the inner outlet with efficiencies surpassing 98%, while the smaller ones were directed towards the outer outlet with efficiencies exceeding 91%. Sample purities of more than 97% and 90% were achieved for 5 μm, and 10 μm particles in the outer and inner outlets, respectively.

The performance of the device was also examined for separating target microparticles from bacteria and its subsequent washing into clean buffer. A separation efficiency of 99.17% was

demonstrated for bacteria in a singleplex samples. Experiments with multiplex samples containing both bacteria and microparticles exhibited a purity of 97.81% and 100% for microparticles collected from the inner outlets and bacteria collected from the outer outlets.

Our proposed device provides simultaneous particle separation and solution exchange for continuous particle washing with potential for use at the point of need. In many applications, our device could be an appropriate alternative to lab-based centrifuges which are bulky and expensive and to membrane filtration systems which are prone to clogging and cell damage. With favorable combinations of passiveness, high throughput, cost-effectiveness, and scalability, this system can become well-suited for various microcentrifugation applications in on-site sample monitoring settings.

CHAPTER 5

Summary and Future Works

5 Summary and Future Works

5.1 Summary

In this study, we demonstrated a multi-layer centrifuge microfluidic device for concurrent separation and washing of particles at high throughputs. This device is applicable when a large volume of sample should be analyzed at point of use or the target particles are rare in the sample. To obtain the high throughput we parallelized a microfluidic device both in-plane and out of plane. We parallelized a total number of 24 curved microchannels in a 3-layer device to enhance the total flowrate of device.

Each microfluidic centrifuge unit integrated Dean flow recirculation of two fluids with selective inertial focusing of target particles. This integration facilitated the isolation of target particles from non-target particles and their subsequent washing into a clean buffer with high throughput and efficiency.

To attain the ultimate flow rate, we divided the process into two distinct phases: in-plane parallelization and out-of-plane parallelization. This approach allowed us to streamline and optimize each aspect independently, enhancing the overall efficiency of the system.

In the first phase solution exchange and particle separation efficiencies were investigated with various flow rates in 2, 4, and 8 curve microchannels with rectangular and polar arrays in one layer. Solution exchange efficiency was measured at the optimum flow rate for devices with polar and rectangular array of microchannels. Results showed that the solution exchange efficiency of collected samples from devices with a rectangular array of microchannels are higher than devices with a polar array of microchannels. We continued our investigation with the rectangular arrayed devices and found the optimum working condition and channel configuration and demonstrated a high throughput, high efficiency particle separation and washing process. We achieved solution exchange efficiencies of > 96.6 % for high flow rates of sample up to 6.4 mL/min. An efficient particle separation was demonstrated at a sample flow rate of 6.4 mL/min for 5 μm, and 10 μm particles, were larger 10 μm particles were separated close to the channel inner wall with efficiencies > 98%. Sample purities of 92.83% and 99.33% were also achieved for 5 μm, and 10 μm particles in the outer and inner outlets, respectively.

During the next phase, we focused on examining the effect of the substrate material (i.e. glass or PDMS) on the efficiency of solution exchange. The transition from glass to PDMS resulted in a slight decrease in the optimized flow rate, shifting from 0.8 mL/min to 0.7 mL/min per curved microchannel for the sample. With these refined flow rates, we observed solution exchange efficiencies of 97.05%, 95.84%, and 96.02% within 2, 4, and 8 curved devices, respectively.

In the next step, we conducted experiments for detailed analyzing of the in-plane parallelized devices that were bonded to a PDMS-covered glass substrate. The results showed high separation

efficiencies, specifically 98.97% and 93.45%, for 10µm and 5µm particles within a 2-curve device. Extending our study to an 8-curve device on a PDMS substrate, we observed similar results with separation efficiencies of 98.97% and 91.64% for 10µm and 5µm particles, respectively. These results approved the effectiveness of our method in achieving high separation efficiency at high throughputs with different particle sizes.

Subsequently, we examined the purity of single-layer devices bonded onto a PDMS substrate. The findings show a high separation purity, with a discerning outcome of 96.2% observed in the inner outlet for particles measuring 10 µm, and an even more impressive separation purity of 98.55% recorded in the outer outlet for particles of 5 µm. These results confirm the efficacy of the utilized methodology in achieving high purity in the separation of particles in a duplex sample, essential for the precise manipulation and separation of particles based on their size.

For further enhancing the device throughput we plasma bonded three layers of the parallelized device and precisely aligned the layers. The final device has a total number of 24 curves interconnected to each other. We demonstrated high throughput and efficiency in separating and washing particles for both singleplex and duplex samples containing one or two distinct sizes of microparticles, respectively. We attained solution exchange efficiencies exceeding 96% at total inlet flow rates of up 16.8 mL/min for multilayer devices.

Efficient particle separation was exhibited at a total inlet flow rate of 16.8 mL/min for both 5 µm and 10 µm particles. The larger 10 µm particles remained near the channel inner wall and were collected from the inner outlet with efficiencies surpassing 98%, while the smaller ones were directed towards the outer outlet with efficiencies exceeding 91%. Sample purities of more than 97% and 90% were achieved for 5 µm, and 10 µm particles in the outer and inner outlets, respectively.

The performance of the device was also examined for separating target microparticles from bacteria and its subsequent washing into clean buffer. A separation efficiency of 99.17% was demonstrated for bacteria in single plex samples. Experiments with multiplex samples containing both bacteria and 10 μm microparticles exhibited a purity of 97.81% and 100% for microparticles collected from the inner outlets and bacteria collected from the outer outlets, respectively.

5.2 Future Works

Our proposed device can potentially provide simultaneous particle separation and solution exchange for continuous particle washing at the point of need. In many applications, our device could be an appropriate alternative to lab-based centrifuges which are bulky and expensive and to membrane filtration systems which are prone to clogging and cell damage. With favorable combinations of passiveness, high throughput, cost-effectiveness, and scalability, this system is well-suited for various microcentrifugation applications in on-site sample monitoring settings.

The limitations of our system may stem from its fabrication method, which relies on photo- and soft-lithography—processes unsuitable for mass production. Exploring faster techniques like micro-milling, 3D printing, or injection molding to manufacture multilayer microcentrifuges from a single material (e.g., glass, PMMA) is favored and warrants further investigation in future research. Utilizing rigid materials can provide more precise alignment and increase the number of layers and the device throughput.

In the presented device we used water as the carrier fluid and clean buffer which are both Newtonian fluids. In many of applications the fluid is non-Newtonian (i.e. blood and milk) where

shear stress plays an important role in manipulation of particles [122]. The application of this device can be extended to non-Newtonian fluids in the future works.

We demonstrated the effect of base substrate on the average Dean velocity while in the proposed correlations in the literature for the average Dean velocity this effect is not accounted for [88], [89]. Further study on the substrate parameters affecting the Dean velocity and revising the current correlation can lead to more accurate and applicable correlation.

Various microchannel dimensions might be designed for different sizes of particles. Also, a cascade sample preparation device might be studied for further steps of manipulation of particles. This device can be integrated with other geometry of microchannels to increase the concentration of rare target particles and multi-step separation of particles.

6 References

[1] Y. Fang, S. Zhu, W. Cheng, Z. Ni, and N. Xiang, "Efficient bioparticle extraction using a miniaturized inertial microfluidic centrifuge," *Lab Chip*, vol. 22, no. 18, pp. 3545–3554, 2022, doi: 10.1039/d2lc00496h.

[2] F. Tian *et al.*, "Protein analysis of extracellular vesicles to monitor and predict therapeutic response in metastatic breast cancer," *Nat. Commun. 2021 121*, vol. 12, no. 1, pp. 1–13, May 2021, doi: 10.1038/s41467-021-22913-7.

[3] M. Ignatiadis, G. W. Sledge, and S. S. Jeffrey, "Liquid biopsy enters the clinic — implementation issues and future challenges," *Nat. Rev. Clin. Oncol. 2021 185*, vol. 18, no. 5, pp. 297–312, Jan. 2021, doi: 10.1038/s41571-020-00457-x.

[4] M. Abbaszadegan, M. S. Huber, C. P. Gerba, and I. L. Pepper, "Detection of enteroviruses in groundwater with the polymerase chain reaction," *Appl. Environ. Microbiol.*, vol. 59, no. 5, pp. 1318–1324, 1993, doi: 10.1128/AEM.59.5.1318-1324.1993.

[5] A. Nikdoost, A. Doostmohammadi, K. Romanick, M. Thomas, and P. Rezai, "Integration of microfluidic sample preparation with PCR detection to investigate the effects of simultaneous DNA-Inhibitor separation and DNA solution exchange," *Anal. Chim. Acta*, vol. 1160, p. 338449, 2021, doi: 10.1016/j.aca.2021.338449.

[6] A. Zabihihesari, A. Khalili, M. J. Farshchi-Heydari, A. Eilaghi, and P. Rezai, "Simple microfluidic device for simultaneous extraction and detection of microplastics in water using DC electrical signal," *New J. Chem.*, vol. 47, no. 19, pp. 9050–9060, May 2023, doi: 10.1039/D2NJ06268B.

[7] K. Zhao *et al.*, "Separation and characterization of microplastic and nanoplastic particles in marine environment," *Environ. Pollut.*, vol. 297, p. 118773, Mar. 2022, doi: 10.1016/J.ENVPOL.2021.118773.

[8] P. Bayat and P. Rezai, "Microfluidic curved-channel centrifuge for solution exchange of target microparticles and their simultaneous separation from bacteria," *Soft Matter*, vol. 14, no. 26, pp. 5356–5363, 2018, doi: 10.1039/C8SM00162F.

[9] D. Yuan *et al.*, "Sheathless separation of microalgae from bacteria using a simple straight channel based on viscoelastic microfluidics," *Lab Chip*, vol. 19, no. 17, pp. 2811–2821, Aug. 2019, doi: 10.1039/C9LC00482C.

[10] F. Wu and C. Dekker, "Nanofabricated structures and microfluidic devices for bacteria: from techniques to biology," *Chem. Soc. Rev.*, vol. 45, no. 2, pp. 268–280, Jan. 2016, doi: 10.1039/C5CS00514K.

[11] D. Abd-El-Haleem, Z. H. Kheiralla, S. Zaki, A. A. Rushdy, and W. Abd-El-Rahiem, "Multiplex-PCR and PCR-RFLP assays to monitor water quality against pathogenic bacteria," *J. Environ. Monit.*, vol. 5, no. 6, pp. 865–870, Nov. 2003, doi: 10.1039/B307476E.

[12] F. Di Nardo, M. Chiarello, S. Cavalera, C. Baggiani, and L. Anfossi, "Ten Years of Lateral Flow Immunoassay Technique Applications: Trends, Challenges and Future Perspectives," *Sensors 2021, Vol. 21, Page 5185*, vol. 21, no. 15, p. 5185, Jul. 2021, doi: 10.3390/S21155185.

[13] Y. Wang, X. Zhang, L. Shang, and Y. Zhao, "Thriving microfluidic technology," *Sci. Bull.*, vol. 66, no. 1, pp. 9–12, Jan. 2021, doi: 10.1016/J.SCIB.2020.07.030.

[14] J. Gong, X. Guo, X. Yan, and C. Hu, “Review of Urban Drinking Water Contamination Source Identification Methods,” *Energies*, vol. 16, no. 2, 2023, doi: 10.3390/en16020705.

[15] B. Wang *et al.*, “Spatial analysis of the influence on ‘microplastic communities’ in the water at a medium scale,” *Sci. Total Environ.*, vol. 885, no. April, 2023, doi: 10.1016/j.scitotenv.2023.163788.

[16] S. R. Chaganti *et al.*, “Variation in the diversity of bacterial communities and potential sources of fecal contamination of beaches in the Huron to Erie corridor,” *Water Res.*, vol. 222, no. February, p. 118913, 2022, doi: 10.1016/j.watres.2022.118913.

[17] S. G. Vrachimis, R. Lifshitz, D. G. Eliades, M. M. Polycarpou, and A. Ostfeld, “Active Contamination Detection in Water-Distribution Systems,” *J. Water Resour. Plan. Manag.*, vol. 146, no. 4, pp. 1–13, 2020, doi: 10.1061/(asce)wr.1943-5452.0001176.

[18] T. S. Hebner and M. A. Maurer-Jones, “Characterizing microplastic size and morphology of photodegraded polymers placed in simulated moving water conditions,” *Environ. Sci. Process. Impacts*, vol. 22, no. 2, pp. 398–407, 2020, doi: 10.1039/c9em00475k.

[19] M. Kooi and A. A. Koelmans, “Simplifying Microplastic via Continuous Probability Distributions for Size, Shape,and Density,” *Environ. Sci. Technol. Lett.*, vol. 6, no. 9, pp. 551–557, 2019, doi: 10.1021/acs.estlett.9b00379.

[20] A. A. Koelmans, N. H. Mohamed Nor, E. Hermsen, M. Kooi, S. M. Mintenig, and J. De France, “Microplastics in freshwaters and drinking water: Critical review and assessment of data quality,” *Water Res.*, vol. 155, pp. 410–422, 2019, doi: 10.1016/j.watres.2019.02.054.

[21] G. Chen, Q. Feng, and J. Wang, “Mini-review of microplastics in the atmosphere and their risks to humans,” *Sci. Total Environ.*, vol. 703, p. 135504, 2020, doi: 10.1016/j.scitotenv.2019.135504.

[22] K. D. Cox, G. A. Covernton, H. L. Davies, J. F. Dower, F. Juanes, and S. E. Dudas, “Human Consumption of Microplastics,” *Environ. Sci. Technol.*, vol. 53, no. 12, pp. 7068–7074, 2019, doi: 10.1021/acs.est.9b01517.

[23] D. Eerkes-Medrano, H. A. Leslie, and B. Quinn, “Microplastics in drinking water: A review and assessment,” *Curr. Opin. Environ. Sci. Heal.*, vol. 7, pp. 69–75, 2019, doi: 10.1016/j.coesh.2018.12.001.

[24] M. Eriksen *et al.*, “Microplastic pollution in the surface waters of the Laurentian Great Lakes,” *Mar. Pollut. Bull.*, vol. 77, no. 1–2, pp. 177–182, 2013, doi: 10.1016/j.marpolbul.2013.10.007.

[25] P. J. Anderson, S. Warrack, V. Langen, J. K. Challis, M. L. Hanson, and M. D. Rennie, “Microplastic contamination in Lake Winnipeg, Canada,” *Environ. Pollut.*, vol. 225, pp. 223–231, 2017, doi: 10.1016/j.envpol.2017.02.072.

[26] S. Lew, K. Glińska-Lewczuk, P. Burandt, M. Grzybowski, and K. Obolewski, “Fecal bacteria in coastal lakes: An anthropogenic contamination or natural element of microbial diversity?,” *Ecol. Indic.*, vol. 152, no. May, 2023, doi: 10.1016/j.ecolind.2023.110370.

[27] P. Marsden *et al.*, “Microplastics in drinking water,” World Health Organization, 1818, WIMEK, , 2019. [Online]. Available: https://edepot.wur.nl/498693

[28] H. De Frond *et al.*, “Monitoring microplastics in drinking water: An interlaboratory study to inform effective methods for quantifying and characterizing microplastics,” *Chemosphere*, vol. 298, no. November 2021, p. 134282, 2022, doi: 10.1016/j.chemosphere.2022.134282.

[29] S. Karimpour Zahraei, A. Salemi, and T. C. Schmidt, “Sample preparation for determination of water taste and odor compounds: A review,” *Trends Environ. Anal. Chem.*, vol. 32, no. July, p. e00149, 2021, doi: 10.1016/j.teac.2021.e00149.

[30] S. Mitra and R. Brukh, *Sample Preparation: An Analytical Perspective*. 2003. doi: 10.1002/0471457817.ch1.

[31] T. B. Billeskov, J. B. Jensen, N. Jessen, and J. Farup, “Fluorescence-activated cell sorting and phenotypic characterization of human fibro-adipogenic progenitors,” *STAR Protoc.*, vol. 4, no. 1, p. 102008, 2023, doi: 10.1016/j.xpro.2022.102008.

[32] B. Schmitz *et al.*, “Magnetic activated cell sorting (MACS) — a new immunomagnetic method for megakaryocytic cell isolation: Comparison of different separation techniques,” *Eur. J. Haematol.*, vol. 52, no. 5, pp. 267–275, 1994, doi: 10.1111/j.1600-0609.1994.tb00095.x.

[33] J. D. Adams, U. Kim, and H. T. Soh, “Multitarget magnetic activated cell sorter,” *Proc. Natl. Acad. Sci. U. S. A.*, vol. 105, no. 47, pp. 18165–18170, 2008, doi: 10.1073/pnas.0809795105.

[34] M. A. Witek, I. M. Freed, and S. A. Soper, “Cell Separations and Sorting,” *Anal. Chem.*, vol. 92, no. 1, pp. 105–131, 2020, doi: 10.1021/acs.analchem.9b05357.

[35] W. S. Low and W. A. B. Wan Abas, “Benchtop technologies for circulating tumor cells separation based on biophysical properties,” *Biomed Res. Int.*, vol. 2015, 2015, doi: 10.1155/2015/239362.

[36] D. W. Fawcett, B. L. Vallee, and M. H. Soule, “A Method for Concentration and Segregation of Malignant Cells from Bloody, Pleural, and Peritoneal Fluids,” *Science (80-.).*, vol. 111, no. 2872, pp. 34–36, Jan. 1950, doi: 10.1126/science.111.2872.34.

[37] E. C. Separation, “and Efficient Cell Separation,” pp. 1–13, 2022.

[38] I. M. Nanoengineered, M. E. Warkiani, A. A. S. Bhagat, B. L. Khoo, J. Han, and C. T. Lim, “Isoporous Micro/Nanoengineered Membranes,” no. 3, pp. 1882–1904, 2013.

[39] W. G. Pitt *et al.*, “Rapid separation of bacteria from blood-review and outlook,” *Biotechnol. Prog.*, vol. 32, no. 4, pp. 823–839, 2016, doi: 10.1002/btpr.2299.

[40] P. Rodriguez-Mateos, B. Ngamsom, C. E. Dyer, A. Iles, and N. Pamme, “Inertial focusing of microparticles, bacteria, and blood in serpentine glass channels,” *Electrophoresis*, vol. 42, no. 21–22, pp. 2246–2255, 2021, doi: 10.1002/elps.202100083.

[41] C. Liu, Q. Feng, and J. Sun, “Lipid Nanovesicles by Microfluidics: Manipulation, Synthesis, and Drug Delivery,” *Adv. Mater.*, vol. 31, no. 45, pp. 1–8, 2019, doi: 10.1002/adma.201804788.

[42] O. N. Katasonova and P. S. Fedotov, “Methods for continuous flow fractionation of microparticles: Outlooks and fields of application,” *J. Anal. Chem.*, vol. 64, no. 3, pp. 212–225, 2009, doi: 10.1134/S1061934809030022.

[43] R. A. Reynolds, D. Stramski, V. M. Wright, and S. B. Woźniak, “Measurements and characterization of particle size distributions in coastal waters,” *J. Geophys. Res. Ocean.*, vol. 115, no. 8, 2010, doi: 10.1029/2009JC005930.

[44] G. Blomquist, “Sampling of biological particles,” *Analyst*, vol. 119, no. 1, pp. 53–56, 1994, doi: 10.1039/AN9941900053.

[45] J. A. Gallego-Urrea, J. Tuoriniemi, and M. Hassellöv, “Applications of particle-tracking analysis to the determination of size distributions and concentrations of nanoparticles in environmental, biological and food samples,” *TrAC - Trends Anal. Chem.*, vol. 30, no. 3, pp. 473–483, 2011, doi:

10.1016/j.trac.2011.01.005.

[46] G. Gharib *et al.*, “Biomedical Applications of Microfluidic Devices: A Review,” *Biosensors*, vol. 12, no. 11, 2022, doi: 10.3390/bios12111023.

[47] A. G. Niculescu, C. Chircov, A. C. Bîrcă, and A. M. Grumezescu, “Fabrication and applications of microfluidic devices: A review,” *Int. J. Mol. Sci.*, vol. 22, no. 4, pp. 1–26, 2021, doi: 10.3390/ijms22042011.

[48] M. Sonker, V. Sahore, and A. T. Woolley, “Recent advances in microfluidic sample preparation and separation techniques for molecular biomarker analysis: A critical review,” *Anal. Chim. Acta*, vol. 986, pp. 1–11, 2017, doi: 10.1016/j.aca.2017.07.043.

[49] A. A. S. Bhagat, H. Bow, H. W. Hou, S. J. Tan, J. Han, and C. T. Lim, “Microfluidics for cell separation,” *Med. Biol. Eng. Comput.*, vol. 48, no. 10, pp. 999–1014, 2010, doi: 10.1007/s11517-010-0611-4.

[50] G. N. M. S, R. Antony, S. Rangabhashiyam, and N. Selvaraju, “Advance approach on environmental assessment and monitoring,” no. December, 2014.

[51] P. Mesquita, L. Gong, and Y. Lin, “Low-cost micro fl uidics : Towards affordable environmental monitoring and assessment,” no. December, pp. 1–23, 2022, doi: 10.3389/frlct.2022.1074009.

[52] Y. Zhang *et al.*, “From passive to active sorting in microfluidics: A review,” *Rev. Adv. Mater. Sci.*, vol. 60, no. 1, pp. 313–324, 2021, doi: 10.1515/rams-2020-0044.

[53] P. Sajeesh and A. K. Sen, “Particle separation and sorting in microfluidic devices: A review,” *Microfluid. Nanofluidics*, vol. 17, no. 1, pp. 1–52, 2014, doi: 10.1007/s10404-013-1291-9.

[54] X. Hu, P. H. Bessette, J. Qian, C. D. Meinhart, P. S. Daugherty, and H. T. Soh, “Marker-specific sorting of rare cells using dielectrophoresis,” *Proc. Natl. Acad. Sci. U. S. A.*, vol. 102, no. 44, pp. 15757–15761, 2005, doi: 10.1073/pnas.0507719102.

[55] L. Wang, J. Lu, S. A. Marchenko, E. S. Monuki, L. A. Flanagan, and A. P. Lee, “Dual frequency dielectrophoresis with interdigitated sidewall electrodes for microfluidic flow-through separation of beads and cells,” *Electrophoresis*, vol. 30, no. 5, pp. 782–791, 2009, doi: 10.1002/elps.200800637.

[56] A. F. Chrimes *et al.*, “Dielectrophoresis-Raman spectroscopy system for analysing suspended nanoparticles,” *Lab Chip*, vol. 11, no. 5, pp. 921–928, 2011, doi: 10.1039/c0lc00481b.

[57] M. Li, S. Li, J. Wu, W. Wen, W. Li, and G. Alici, “A simple and cost-effective method for fabrication of integrated electronic-microfluidic devices using a laser-patterned PDMS layer,” *Microfluid. Nanofluidics*, vol. 12, no. 5, pp. 751–760, 2012, doi: 10.1007/s10404-011-0917-z.

[58] J. Voldman, M. Toner, M. L. Gray, and M. A. Schmidt, “A Dielectrophoresis-based Array Cytometer,” *Transducers ’01 Eurosensors XV*, pp. 322–325, 2001, doi: 10.1007/978-3-642-59497-7_76.

[59] R. Martinez-Duarte, P. Renaud, and M. J. Madou, “A novel approach to dielectrophoresis using carbon electrodes,” *Electrophoresis*, vol. 32, no. 17, pp. 2385–2392, 2011, doi: 10.1002/elps.201100059.

[60] C. Iliescu, G. L. Xu, V. Samper, and F. E. H. Tay, “Fabrication of a dielectrophoretic chip with 3D silicon electrodes,” *J. Micromechanics Microengineering*, vol. 15, no. 3, pp. 494–500, 2005, doi: 10.1088/0960-1317/15/3/009.

[61] T. Zhang *et al.*, “Focusing of sub-micrometer particles in microfluidic devices,” *Lab Chip*, vol. 20, no. 1, pp. 35–53, 2020, doi: 10.1039/c9lc00785g.

[62] G. Destgeer, B. H. Ha, J. H. Jung, and H. J. Sung, “Submicron separation of microspheres via travelling surface acoustic waves,” *Lab Chip*, vol. 14, no. 24, pp. 4665–4672, 2014, doi: 10.1039/c4lc00868e.

[63] K. Lee, H. Shao, R. Weissleder, H. Lee, and L. E. E. E. T. Al, “Acoustic Puri fi cation of Extracellular Microvesicles,” no. 3, pp. 2321–2327, 2015.

[64] R. Wang, S. Sun, W. Wang, and Z. Zhu, “Investigation on the thermophoretic sorting for submicroparticles in a sorter with expansion-contraction microchannel,” *Int. J. Heat Mass Transf.*, vol. 133, pp. 912–919, 2019, doi: 10.1016/j.ijheatmasstransfer.2018.12.126.

[65] R. Wang, J. Du, W. Guo, and Z. Zhu, “Investigation on the thermophoresis-coupled inertial sorting of submicrometer particles in a microchannel,” *Nanoscale Microscale Thermophys. Eng.*, vol. 20, no. 1, pp. 51–65, 2016, doi: 10.1080/15567265.2015.1124159.

[66] S. A. Peyman, A. Iles, and N. Pamme, “Rapid on-chip multi-step (bio)chemical procedures in continuous flow - Manoeuvring particles through co-laminar reagent streams,” *Chem. Commun.*, no. 10, pp. 1220–1222, 2008, doi: 10.1039/b716532c.

[67] S. I. Han *et al.*, “Identification of Microorganisms that Bind Specifically to Target Materials of Interest Using a Magnetophoretic Microfluidic Platform,” *ACS Appl. Mater. Interfaces*, vol. 15, no. 9, pp. 11391–11402, 2023, doi: 10.1021/acsami.2c15192.

[68] L. R. Huang, E. C. Cox, R. H. Austin, and J. C. Sturm, “Continuous Particle Separation Through Deterministic Lateral Displacement,” *Science (80-.).*, vol. 304, no. 5673, pp. 987–990, 2004, doi: 10.1126/science.1094567.

[69] B. M. Dincau, A. Aghilinejad, T. Hammersley, X. Chen, and J. H. Kim, “Deterministic lateral displacement (DLD) in the high Reynolds number regime: high-throughput and dynamic separation characteristics,” *Microfluid. Nanofluidics*, vol. 22, no. 6, pp. 1–8, 2018, doi: 10.1007/s10404-018-2078-9.

[70] M. Rahmati and X. Chen, “Separation of circulating tumor cells from blood using dielectrophoretic DLD manipulation,” *Biomed. Microdevices*, vol. 23, no. 4, 2021, doi: 10.1007/s10544-021-00587-8.

[71] J. M. Martel and M. Toner, “Inertial focusing in microfluidics,” *Annu. Rev. Biomed. Eng.*, vol. 16, pp. 371–396, 2014, doi: 10.1146/annurev-bioeng-121813-120704.

[72] J. Zhang *et al.*, “Fundamentals and applications of inertial microfluidics: A review,” *Lab Chip*, vol. 16, no. 1, pp. 10–34, 2016, doi: 10.1039/c5lc01159k.

[73] V. Kumar and P. Rezai, “Multiplex Inertio-Magnetic Fractionation (MIMF) of magnetic and non-magnetic microparticles in a microfluidic device,” *Microfluid. Nanofluidics*, vol. 21, no. 5, pp. 1–14, 2017, doi: 10.1007/s10404-017-1919-2.

[74] D. Di Carlo, D. Irimia, R. G. Tompkins, and M. Toner, “Continuous inertial focusing, ordering, and separation of particles in microchannels,” *Proc. Natl. Acad. Sci. U. S. A.*, vol. 104, no. 48, pp. 18892–18897, 2007, doi: 10.1073/pnas.0704958104.

[75] S. C. Hur, T. Z. Brinckerhoff, C. M. Walthers, J. C. Y. Dunn, and D. Di Carlo, “Label-Free Enrichment of Adrenal Cortical Progenitor Cells Using Inertial Microfluidics,” *PLoS One*, vol. 7, no. 10, 2012, doi: 10.1371/journal.pone.0046550.

[76] D. R. Gossett *et al.*, “Inertial manipulation and transfer of microparticles across laminar fluid streams,” *Small*, vol. 8, no. 17, pp. 2757–2764, 2012, doi: 10.1002/smll.201200588.

[77] J. S. Dudani, D. E. Go, D. R. Gossett, A. P. Tan, and D. Di Carlo, “Mediating millisecond reaction time around particles and cells,” *Anal. Chem.*, vol. 86, no. 3, pp. 1502–1510, 2014, doi: 10.1021/ac402920m.

[78] J. Zhou, P. V. Giridhar, S. Kasper, and I. Papautsky, “Modulation of aspect ratio for complete separation in an inertial microfluidic channel,” *Lab Chip*, vol. 13, no. 10, pp. 1919–1929, 2013, doi: 10.1039/c3lc50101a.

[79] J. Zhang *et al.*, “Fundamentals and applications of inertial microfluidics: A review,” *Lab on a Chip*, vol. 16, no. 1. 2016. doi: 10.1039/c5lc01159k.

[80] D. Di Carlo, “Inertial microfluidics,” *Lab Chip*, vol. 9, no. 21, pp. 3038–3046, 2009, doi: 10.1039/b912547g.

[81] M. S. Islam and X. Chen, “Continuous CTC separation through a DEP-based contraction–expansion inertial microfluidic channel,” *Biotechnol. Prog.*, vol. 39, no. 4, pp. 1–15, 2023, doi: 10.1002/btpr.3341.

[82] S. Ebrahimi, M. Alishiri, E. Pishbin, H. Afjoul, and A. Shamloo, “A curved expansion-contraction microfluidic structure for inertial based separation of circulating tumor cells from blood samples,” *J. Chromatogr. A*, vol. 1705, p. 464200, 2023, doi: 10.1016/j.chroma.2023.464200.

[83] S. Shen, X. Wang, and Y. Niu, “Multi-vortex regulation for efficient fluid and particle manipulation in ultra-low aspect ratio curved microchannels,” *Micromachines*, vol. 12, no. 7, 2021, doi: 10.3390/mi12070758.

[84] Y. K. Hahn, D. Hong, J. H. Kang, and S. Choi, “A reconfigurable microfluidics platform for microparticle separation and fluid mixing,” *Micromachines*, vol. 7, no. 8, pp. 1–10, 2016, doi: 10.3390/mi7080139.

[85] H. M. AU - Tay, D. C. AU - Yeo, C. AU - Wiraja, C. AU - Xu, and H. W. AU - Hou, “Microfluidic Buffer Exchange for Interference-free Micro/Nanoparticle Cell Engineering,” *JoVE*, no. 113, p. e54327, 2016, doi: doi:10.3791/54327.

[86] H. Ramachandraiah *et al.*, “Dean flow-coupled inertial focusing in curved channels,” *Biomicrofluidics*, vol. 8, no. 3, 2014, doi: 10.1063/1.4884306.

[87] J. M. Ottino and S. Wiggins, “Introduction: Mixing in microfluidics,” *Philos. Trans. R. Soc. A Math. Phys. Eng. Sci.*, vol. 362, no. 1818, pp. 923–935, 2004, doi: 10.1098/rsta.2003.1355.

[88] S. Ookawara, R. Higashi, D. Street, and K. Ogawa, “Feasibility study on concentration of slurry and classification of contained particles by microchannel,” *Chem. Eng. J.*, vol. 101, no. 1–3, pp. 171–178, 2004, doi: 10.1016/j.cej.2003.11.008.

[89] P. Bayat and P. Rezai, “Semi-Empirical Estimation of Dean Flow Velocity in Curved Microchannels,” *Sci. Rep.*, vol. 7, no. 1, pp. 1–13, 2017, doi: 10.1038/s41598-017-13090-z.

[90] J. M. Martel and M. Toner, “Inertial focusing dynamics in spiral microchannels,” *Phys. Fluids*, vol. 24, no. 3, 2012, doi: 10.1063/1.3681228.

[91] N. Nivedita, P. Ligrani, and I. Papautsky, “Spiral inertial microfluidic devices for continuous blood cell separation,” *Microfluid. BioMEMS, Med. Microsystems X*, vol. 8251, no. February 2012, p. 82510R, 2012, doi: 10.1117/12.909936.

[92] W. Pakhira, R. Kumar, and K. M. Ibrahimi, “Distinct separation of multiple CTCs using inertial focusing phenomena utilizing single-looped spiral microfluidic lab-on-chip,” *Chem. Eng. Sci.*, vol. 275, p. 118724, 2023, doi: 10.1016/j.ces.2023.118724.

[93] J. Zhang, S. Yan, W. Li, G. Alici, and N. T. Nguyen, “High throughput extraction of plasma using a secondary flow-aided inertial microfluidic device,” *RSC Adv.*, vol. 4, no. 63, pp. 33149–33159, 2014, doi: 10.1039/c4ra06513a.

[94] J. Zhang, M. Li, W. H. Li, and G. Alici, “Inertial focusing in a straight channel with asymmetrical expansion-contraction cavity arrays using two secondary flows,” *J. Micromechanics Microengineering*, vol. 23, no. 8, 2013, doi: 10.1088/0960-1317/23/8/085023.

[95] G. Guan *et al.*, “Spiral microchannel with rectangular and trapezoidal cross-sections for size based particle separation,” *Sci. Rep.*, vol. 3, pp. 1–9, 2013, doi: 10.1038/srep01475.

[96] S. Shen *et al.*, “Ultra-low aspect ratio spiral microchannel with ordered micro-bars for flow-rate insensitive blood plasma extraction,” *Sensors Actuators, B Chem.*, vol. 287, no. December 2018, pp. 320–328, 2019, doi: 10.1016/j.snb.2019.02.066.

[97] A. Mihandoust, S. R. Bazaz, N. Maleki-Jirsaraei, M. Alizadeh, R. A. Taylor, and M. E. Warkiani, “High-throughput particle concentration using complex cross-section microchannels,” *Micromachines*, vol. 11, no. 4, 2020, doi: 10.3390/MI11040440.

[98] A. J. Mach and D. di Carlo, “Continuous scalable blood filtration device using inertial microfluidics,” *Biotechnol. Bioeng.*, vol. 107, no. 2, pp. 302–311, 2010, doi: 10.1002/bit.22833.

[99] M. E. Warkiani, A. K. P. Tay, G. Guan, and J. Han, “Membrane-less microfiltration using inertial microfluidics,” *Sci. Rep.*, vol. 5, pp. 1–10, 2015, doi: 10.1038/srep11018.

[100] M. Rafeie, J. Zhang, M. Asadnia, W. Li, and M. E. Warkiani, “Multiplexing slanted spiral microchannels for ultra-fast blood plasma separation,” *Lab Chip*, vol. 16, no. 15, pp. 2791–2802, 2016, doi: 10.1039/c6lc00713a.

[101] Y. Fang, S. Zhu, W. Cheng, Z. Ni, and N. Xiang, “Efficient bioparticle extraction using a miniaturized inertial microfluidic centrifuge,” *Lab Chip*, vol. 22, no. 18, pp. 3545–3554, 2022, doi: 10.1039/d2lc00496h.

[102] T. Zhang *et al.*, “Focusing of sub-micrometer particles in microfluidic devices,” *Lab Chip*, vol. 20, no. 1, pp. 35–53, 2020, doi: 10.1039/c9lc00785g.

[103] D. Yuan *et al.*, “Dean-flow-coupled elasto-inertial particle and cell focusing in symmetric serpentine microchannels,” *Microfluid. Nanofluidics*, vol. 23, no. 3, pp. 1–9, 2019, doi: 10.1007/s10404-019-2204-3.

[104] S. Narayana Iyengar, T. Kumar, G. Mårtensson, and A. Russom, “High resolution and rapid separation of bacteria from blood using elasto-inertial microfluidics,” *Electrophoresis*, vol. 42, no. 23, pp. 2538–2551, 2021, doi: 10.1002/elps.202100140.

[105] A. Nikdoost and P. Rezai, “Microparticle manipulation in viscoelastic flows inside curvilinear microchannels: a thorough fundamental study with application to simultaneous particle sorting and washing,” *New J. Chem.*, vol. 47, no. 4, pp. 1635–1648, 2022, doi: 10.1039/d2nj05328d.

[106] A. A. S. Bhagat, S. S. Kuntaegowdanahalli, and I. Papautsky, “Inertial microfluidics for continuous particle filtration and extraction,” *Microfluid. Nanofluidics*, vol. 7, no. 2, pp. 217–226, 2009, doi: 10.1007/s10404-008-0377-2.

[107] S. D. Hudson, “Poiseuille flow and drop circulation in microchannels,” *Rheol. Acta*, vol. 49, no. 3, pp. 237–243, 2010, doi: 10.1007/s00397-009-0394-4.

[108] H. Bruus, *Theoretical Microfluidics*. 2008. doi: 10.1093/oso/9780199235087.001.0001.

[109] E. Infeld, A. Karczewska, G. Rowlands, and P. Rozmej, “Exact cnoidal solutions of the extended KdV equation,” *Acta Phys. Pol. A*, vol. 133, no. 5, pp. 1191–1199, 2018, doi: 10.12693/APhysPolA.133.1191.

[110] *Fundamentals of heat and mass transfer*. Sixth edition / [Frank P. Incropera ... [and others]. Hoboken, NJ : John Wiley, [2007] ©2007. [Online]. Available: https://search.library.wisc.edu/catalog/9910020981602121

[111] T. Werner and E. Lobach, “Photolithographic method for the manufacture of integrated circuits,” no. 19, 1982.

[112] D. SU8-2000, “Su-8 2025-75,” *2025, 2035, 2050, 2075*, pp. 1–5, 2006, [Online]. Available: papers3://publication/uuid/E7A575F7-4BEF-4981-8E02-277673CABC12

[113] D. Qin, Y. Xia, and G. M. Whitesides, “Soft lithography for micro- and nanoscale patterning,” *Nat. Protoc.*, vol. 5, no. 3, pp. 491–502, 2010, doi: 10.1038/nprot.2009.234.

[114] “Practical Handbook of Microbiology - Google Books.”

[115] C. A. Schneider, W. S. Rasband, and K. W. Eliceiri, “NIH Image to ImageJ: 25 years of image analysis,” *Nat. Methods*, vol. 9, no. 7, pp. 671–675, 2012, doi: 10.1038/nmeth.2089.

[116] P. Bayat and P. Rezai, “Microfluidic curved-channel centrifuge for solution exchange of target microparticles and their simultaneous separation from bacteria,” *Soft Matter*, vol. 14, no. 26, pp. 5356–5363, 2018, doi: 10.1039/C8SM00162F.

[117] S. Razavi Bazaz *et al.*, “Zigzag microchannel for rigid inertial separation and enrichment (Z-RISE) of cells and particles,” *Lab Chip*, vol. 22, no. 21, pp. 4093–4109, Oct. 2022, doi: 10.1039/D2LC00290F.

[118] B. W. Peterson, P. K. Sharma, H. C. van der Mei, and H. J. Busscher, “Bacterial Cell Surface Damage Due to Centrifugal Compaction,” *Appl. Environ. Microbiol.*, vol. 78, no. 1, p. 120, Jan. 2012, doi: 10.1128/AEM.06780-11.

[119] D. Rodoplu Solovchuk, I. H. Boyaci, U. Tamer, N. Sahiner, and D. Cetin, “A simple gradient centrifugation method for bacteria detection in skim milk,” *Microchem. J.*, vol. 189, p. 108479, Jun. 2023, doi: 10.1016/J.MICROC.2023.108479.

[120] H. W. Hou, R. P. Bhattacharyya, D. T. Hung, and J. Han, “Direct detection and drug-resistance profiling of bacteremias using inertial microfluidics,” *Lab Chip*, vol. 15, no. 10, pp. 2297–2307, 2015, doi: 10.1039/c5lc00311c.

[121] A. Andino and I. Hanning, “Salmonella enterica: Survival, colonization, and virulence differences among serovars,” *Sci. World J.*, vol. 2015, no. Table 3, 2015, doi: 10.1155/2015/520179.

[122] D. J. Lee, H. Brenner, J. R. Youn, and Y. S. Song, “Multiplex particle focusing via hydrodynamic force in Viscoelastic Fluids,” *Sci. Rep.*, vol. 3, pp. 3–10, 2013, doi: 10.1038/srep03258.